Generalized Solutions to Several Problems in Open Channel Hydraulics

2021

MEAN Sovanna

Table of Contents

Notations

Symbols

A	Cross-sectional area
A_0	Initial cross-sectional area at $t = 0$
B_1	Bottom width
$C(u_l, u_r)$	Local celerity at a jump from u_l to u_r
F	Flux
F_s	Specific force
Fr	Froude number
g	Acceleration due to gravity
H	Hamiltonian
h	Water depth
h^{up}	Upstream water depth
h_{cri}	Critical flow depth
h_{uni}	Uniform flow depth
M	Parameter controlling singular viscosity regularization
n	Manning's roughness
P	Wetted perimeter
p_1	u_x as an argument of Hamiltonian
p	An exponent of the friction law
Q	Discharge
Q_{f}	The numerical flux of discharge
Q_{in}	Inflow discharge

Q_L	A flux of discharge in the left-side cell
Q_{out}	Outflow discharge
Q_R	A flux of discharge in the right-side cell
q	Lateral inflow discharge per unit width
R	Hydraulic radius
r	Source term
S_{cri}	Slope at critical flow depth
S_f	Friction slope
S_0	Bed slope
t	Time
u	Unknown variable
u_{cri}	Unknown variable for critical flow depth
u_{down}	Unknown variable for downstream water depth
u_l	u at the left-hand side of a jump
u_r	u at the right-hand side of a jump
u_{uni}	Unknown variable for uniform flow depth
u_{up}	Unknown variable for upstream water depth
V	Cross-sectional averaged velocity
x	Local curvilinear abscissa along the channel bed or Space coordinate
z	Upward vertical axis
Z_b	Bed elevation
β	Momentum coefficient
γ	Parameter to approximate singular diffusion
η	Water level
ξ	x at the previous time stage
$\phi = \phi(t, x, z)$	Level-set function as a function of t, x, and z

$\hat{\phi}$	Interpolated ϕ
ψ	Singular viscosity term
ΔQ_{Mj}	The maximum increments of discharge within time steps

Subscripts

k, i, j	Integers indexing discretized t, x, z
L	Left-side cell
R	Right-side cell
x	Partial derivative with respect to x
z	Partial derivative with respect to z

Prefix

Δ	Increment

Spaces

C	The space of continuous function
C_B	The space of all continuous function, including first derivatives
C^1	The space of all infinitely differentiable function
C_B^1	The space of all bounded and continuous function, including first derivatives
C^∞	The space of all infinitely differentiable function
L^1	Lebesgue space of all integrable functions
L^∞	Lebesgue spaces
LSC	The space of lower semi-continuous functions
$\mathbb{R}$	The set of real numbers
USC	The space of upper semi-continuous functions
$W^{1,1}$	Sobolev space with the norm $\|\bullet\|_{1,1}$

$W^{1,\infty}$	Sobolev space with the norm $\|\bullet\|_{1,\infty}$
$\mathbb{Z}$	The set of integers

Abbreviations

CDL	Critical-depth line
FOQL PDE	First-order quasilinear partial differential equation
GS	Generalized solution
GVFS	Gradually varied flow solution
HJ equation	Hamilton-Jacobi equation
L-env	Lower semi-continuous envelope
SFO ODE	Scalar first-order ordinary differential equation
sub-S	Viscosity sub-solution
super-S	Viscosity super-solution
SVR	Singular viscosity regularization
SWEs	Shallow water equations
U-env	Upper semi-continuous envelope
UDL	Uniform-depth line
VS	Viscosity solution

List of Figures

List of Tables

Acknowledgements

The author would like to express her sincere appreciation to Dr. Masayuki FUJIHARA, Professor of Water Resources Engineering, Division of Environmental Science and Technology, Graduate School of Agriculture, Kyoto University, for his courteous advice and helps during the research.

The author gratefully acknowledges and expresses the most profound gratitude to her adviser Dr. Koichi UNAMI, Associated Professor of Water Resources Engineering Laboratory, for his courteous advice, encouragement, and untiring help during the research period.

The author would like to thank Dr. Junichiro TAKEUCHI, Assistant Professor of Water Resources Engineering Laboratory, for his valuable comments and suggestions.

The author would like to thank Dr. Hisashi OKAMOTO, Professor in Department of Mathematics, Gakushuin University, Japan, for conceptual, review, and editing Chapter 5 of this thesis.

Gratefully thanks all Water Resources Engineering Laboratory members with special extend to Mrs. Ishida and Ms. Nana Fuchino, secretaries of the Laboratory, for their assistance and cooperation.

Finally, the author wishes to express her special gratitude to her family members and friends for their untiring and unending support, enabling her to complete the study successfully.

May 25th, 2021

MEAN Sovanna

Chapter 1

1 Introduction

1.1 Open channel flows

Open channel flows are the flows having free surfaces that are subject to atmospheric pressure. The flow whose depth varies gradually and steadily along the length of the channel is called a gradually varied flow (GVF). In contrast, the abrupt change in curvature of the flow profiles is called a rapidly varied flow (RVF). GVF bases on the energy equation, and RVF bases on the momentum equation. The abrupt change in the flow profiles results in a discontinuous profile called the hydraulic jump or shock in RVF. The open channel flows include the flows in the rivers, canals, lakes, channels, and sewer systems if they have the free surface.

The solutions of the open channel flows are determined to address a particular issue in hydrology, hydraulics, and engineering. Computational simulations are required, including

computer techniques, informatics, and numerical methods to obtain the solutions of the flows [1]. There are two types of computational simulations: non-physical-based models and physical-based models. Non-physical-based models are black-box type models, which require calibration of input parameters. On the other hand, physical-based models are numerical models based on mathematical aspects to describe the open channel flows by differential equations, and it requires either fewer parameters or no calibration. In mathematical and numerical modeling, the open channel flow is usually characterized by a 1-dimensional (1D) model of shallow water equations (SWEs) or Saint-Venant equations, which is reasonably easy to solve compared to a multi-dimensional model. The SWEs in steady states comprehend RVF, including GVF.

1.2 Research issues

The essential requirement of the treatment of wet and dry beds is to keep water depth greater than zero to make SWEs achieve a stable numerical solution [2]. There is no problem with a wet bed; however, it remains a difficulty and an interest in treating a dry bed. The numerical computation may fail, and it introduces no physical negative water depth [3,4] when the initial water depth is precisely zero. The dry bed is defined by inputting a sufficiently small water depth in most numerical simulations such that the dry domain was treated as the wet bed [4]. Hence, the way to treat the dry bed arises when the initial water depth is exactly zero. The treatment of the dry bed in the open channel flows is the first issue.

Modeling open channel flows with discontinuities has been a great challenge to hydraulic researchers and engineers [4]. The second issue is a misunderstanding that a discontinuity of the kinematic wave develops because of the discontinuity of initial input data. In addition, the wave dissipates over time. Singh [5] stated that shock could occur in the kinematic wave model when there was an abrupt change in rainfall intensity, bed roughness, bed elevation, etc. The occurrence of the shock would dissipate as time went by. Nevertheless, the first-order quasilinear partial differential equations (FOQL PDEs), including the kinematic wave model, admit discontinuities from discontinuous initial input data and smooth input data. Furthermore, the generalized solutions (GSs) do not dissipate with time.

Enormous efforts have been placed on initial-boundary value problems of the SWEs for the numerical solutions of unsteady flows to investigate surface water flows. The 1D SWEs are the hyperbolic system. One should notice that the hyperbolic system, in general, is a function with bounded variations, possibly with a countable number of discontinuities. In hydraulic design, open channel flow in a steady state is required. The SWEs become a scalar first-order ordinary differential equation (SFO ODE) when the unsteady terms are dropped. The SFO ODE with an initial condition known as the initial value problem has been studied. On the other hand, the SFO ODE with Dirichlet boundary condition known to be an ill-posed problem remains a little-discussed topic. In general, the ill-posed problem is a highly nontrivial matter to prove the existence, uniqueness, and stability. Hence, the last issue is how to describe characteristics of possibly GSs to Dirichlet problems of the SFO ODE.

1.3 Research objectives

This thesis aims to provide mathematical and numerical modeling in locally 1D open channel flows to deal with the research issues. The thesis anticipates the model of full dynamics and the approximation of the SWEs, mathematical proof of the GSs, and the numerical modeling for approximating the solutions. The thesis proposes the following topics to achieve the research objectives:

1) application of level-set methods to the kinematic wave equation in the open channel flows,
2) numerical demonstrations of non-dissipative discontinuous kinematic waves in the open channel flows,
3) a thorough description of one-dimensional steady open channel flows using the notion of discontinuous viscosity solution (VS).

1.4 Structure of the thesis

The organization of this thesis is as follows.

In Chapter 1, the general idea of open channel flows, research issues, and research objectives are stated.

In Chapter 2, literature reviews on related topics will be provided, including the applicability of SWEs to hydro-environmental problems, the applicability of the kinematic wave equation, treatment of dry bed, discontinuities of water surface profile, and VS involving hydraulic jump.

In Chapter 3, level-set methods applied to the kinematic wave equation governing open channel flows are discussed. The kinematic wave equation is regarded as a Hamilton-Jacobi equation (HJ equation). The computed zeros of the level-set function represent the water depths. However, the solutions develop overturning phenomena. Singular viscosity regularization (SVR) is implemented to reduce the effects of the overturning phenomena. Finally, a testing of abrupt water release from Chan Thnal Reservoir to its irrigation canal with varied bed slopes in the dry bed condition is simulated, serving as a practical demonstration.

In Chapter 4, numerical examples of the non-dissipative discontinuous kinematic wave model in open channels are presented to clarify that a discontinuity can develop without dissipation under the smoothness of all input. Unlike Chapter 3, the kinematic wave equation is considered a FOQL PDE and then a Cauchy problem. The GS to the Cauchy problem is described. Two cases of numerical examples for discontinuous initial data and smooth initial data are computed using the Godunov scheme. The non-dissipative discontinuous waves are analyzed for the case of smooth initial data.

In Chapter 5, a study on a thorough description of one-dimensional steady open channel flows using the notion of VS is discussed. The chapter gives detail of problem formulation and mathematical analysis of 1D steady flows with the unique existence of GVFSs. Then, the notion of discontinuous VS is employed to prove the non-uniqueness of GSs. Finally, illustrative examples are demonstrated.

To sum up, in Chapter 6, a summary and future works of this thesis are provided.

Chapter 2

2 Literature review

2.1 Applicability of SWEs to hydro-environmental problems

Hydro-environmental problems are one of the fields that SWEs applicable to use to understand flow variables. A better understanding of flow variables enables decision-makers to control flow, minimize wasteful drained water at unnecessary periods, and protect strategic infrastructure and hydraulic structures. It would benefit for preserving agricultural areas, managing water resources, and ensuring water supply along with the canal system, which could avoid water issues between upstream and downstream [6].

The SWEs have been seen in various forms of dimensions: (1D) rivers, channels, sewer system and (2D) seas, rivers, overland flows [7]. The open channel flows are related to hydraulic research and engineering fields in terms of flows in the rivers, canals, lakes, channels, and sediment transport in the 1D system [9–16]. Kesserwani and Liang [8] studied

the 1D SWEs using the second-order Runge–Kutta discontinuous Galerkin scheme considering wet and dry bed over the complex topography. Burguete *et al*. [9] proposed friction term discretization and limitation in 1D SWEs to some applications of a dam-break flow problem in a mountain river, unsteady flow with experimental data, tsunami propagating model, and surface irrigation flow. Cao *et al*. [10] presented dam-break flows and sediment transport mechanics over the mobile bed. A morphodynamical modeling system is typically concerned with a hydrodynamic component. It describes the flow dynamics and a sediment transport or morphological component for the bed evolution [11]. Kalita [12] studied a coupled morphodynamical flow model of SWEs and Exner equation using a TVD MacCormack scheme to simulate dynamic flow processes. The model tested different bed conditions, including bed aggradation, bed degradation, dam-break flow over the erodible bed, and movable bumps. It produced excellent results for wavefronts of water surface flow and sediment. The model of leaky barriers in the channel system has studied the impact and reduce flooding risk. The roles of the leaky obstacles are to decrease high flows and temporarily store water on the floodplain [13]. Lai et al. [14] conducted a study on the impacts of lake inflow and the Yangtze River on Poyang Lake level during two time periods: the rising and falling flood stages in May and October. To study the hydrodynamic processes of the lake, they integrated 1D SWEs and 2D SWEs. Tinti and Tonini [15] identified analytical solutions of SWEs and an amplification factor of the tsunami height. They indicated that the amplification specified the epicenter of tsunamic-inducing earthquake weather in the land or sea. Kobayashi and Takara [16] developed a distribution of rainfall-run-off/flood-inundation simulation model based on 1D SWEs for river routing and 2D SWEs for surface flow and

then cooperated with an economic risk assessment model. The model focused on the rainfall-runoff processes and inland or dike-break inundation processes.

2.2 Applicability of the kinematic wave equation

The development of kinematic wave theory by Lighthill and Whitham [17] has been widely used in water resources [19–24] and traffic flows [24]. The theory applies to various water resources, specifically hydrological processes, overland flow, open channel flow, base flow, unsaturated flow, macropore flow, river hydraulics, movement glaciers, erosion, and sediment transport. Singh and de Lima [18] derived the analytical solutions of 1D kinematic wave approximation to visualize the overland flow moving downstream and a storm moving upstream of characteristics. Chen and Capart [19] proposed the kinematic wave model to simulate dam-break floods. The model gives advantages of low computational cost, real-time forecast, and limited data. Liu and Singh [20] focused on the overland flow on a hillslope using a 1D kinematic wave model. The overland flow was impacted by microtopography, slope length and gradient, and vegetative cover. Even though the solutions of overland flow may ideally be derived from SWEs, the kinematic wave approximation could produce very reliable results for overland flow and other hydrological models, and it is recognized for its fast and accurate solutions [21]. Kinematic wave theory is used to model the overland flow. Explicit finite difference approximations with the analytical method of characteristics are made to the kinematic wave model to account for the spatial and temporal distribution of the rainfall and variable boundary conditions [25]. Howes *et al*. [22] addressed two distribution models, 1D and 2D kinematic wave models, to simulate overland flow in two semiarid

shrubland watersheds in the Jornada Basin, New Mexico. 1D and 2D kinematic wave models were computed the flow volume of a fixed network and flow directions, respectively. Isidoro and de Lima [23] presented the solutions of the 1D linear kinematic wave equation to evaluate the discharge over the total drainage plane surface under the moving rainstorms. The results are compared among the analytical solutions, numerical solutions, and experimental solutions at the laboratory. Jin [24] described the dynamics traffic of lane-changing in the framework of the kinematic wave theory. Jin stated that lane-changing intensities highly depended on road geometry, location, on-ramp/off-ramp traffic, lane-changing time, vehicle speeds, and other traffic conditions.

2.3 Treatment of dry bed

Many papers have been discussed the wetting and drying conditions [2, 9, 27–29]. The initial water depth of the dry bed is specified as 10^{-5} (m) [3], 10^{-7} (m) [4], 10^{-8} (m) [29], or less than 10^{-8} (m) [8]. Kesserwani and Liang [8] analyzed the 1D SWEs using the second-order Runge–Kutta discontinuous Galerkin scheme considering wet and dry bed over the complex topography. Han and Warnecke [26] determined the Riemann solutions to the SWEs with the dry bed problem. They focused on two cases of dry bed problems. One was the case that the water propagated to the left or right dry bed. The second was the dry bed appeared because of the flow motions. Bunya *et al*. [2] assessed the piecewise linear Runge–Kutta discontinuous Galerkin approximation to the SWEs for wetting and drying treatment. In addition, a little positivity of water depth is applied in the numerical flux computation to prevent instability due to excessive drying. Alias *et al*. [27] presented the open channel flows

using a 1D well-balanced finite volume Godunov-type scheme involving wetting and drying phenomena. Hernandez-Duenas and Beljadid [3] proposed a semi-discrete central-upwind scheme for shallow-water flows. They discussed the analytical solutions to numerical solutions and laboratory results in the cases of wetting and drying. Ern *et al*. [28] analyzed the performance of the 1D and 2D SWEs and introduced a flux modification technique and slope modification technique to deal with wetting and drying fronts. All these papers considered a sufficiently small positive value of the initial water depth as the dry bed condition.

2.4 Discontinuities of water surface profile

Discontinuities of surface water flows, namely hydraulic jumps or shocks, are formed whenever there are rapid changes of supercritical flows to subcritical flows. Hydraulic jumps are a challenging topic for hydraulic and environmental engineering due to their complicated nature, unsteady and high-level turbulence, and air entrainment.

Hydraulic jumps are common phenomena that have been generally found in natural and artificial open channel flows [30]. Various studies of hydraulic jumps have been conducted to approximate and understand their flow phenomena. Chow [31] computed the water surface profiles for the subcritical flow starting from the downstream end and the supercritical flow starting from the upstream end to determine the jump location. The jump is formed at a location where the specific forces on the left and right of the jump are equivalent [32]. Carrillo *et al*. [33] conducted experiments to observe the characteristics of the air-water flow of five submerged hydraulic jumps generated downstream of rectangular

falling jets. Harada and Li [34] modeled the hydraulic jumps using the bubbly two-phase flow method, which applied the Reynolds-averaged Navier–Stokes equations. The model investigated air entrainment, turbulent shear stress, and interaction between flow structures and the bottom shear stress in the jump to understand the air-water flow better.

2.5 VS involving hydraulic jump

The HJ equation is known to engineers and physicists as a partial differential equation (PDE) which arises in the study of mechanics, yielding solutions of a system of ordinary differential equations. It is also known through its relation to control theory, differential games, or other optimization [35]. Due to the highly nonlinear form of the equation, classical solutions (smooth) cannot be expected to exist [36]. Thus, the notion of VSs gains attention.

This section attempts to briefly introduce the VSs of first-order PDE and review some aspects of the solutions. The notion of VS to first order fully nonlinear equations was primarily introduced by Crandall and Lions [37], in which the notion has been widely accepted as the correct notion of GSs. The VS is a general classical concept of solution to PDE. It has been realized that the VS is a natural solution that has contributed to many applications of PDE, including first-order equations in dynamic programming (the Hamilton-Jacobi-Bellman equation), differential games (the Hamilton-Jacobi-Issacs equation), front evolution problems, and the ones in stochastic optimal control.

The VS has two types: continuous and discontinuous VS. The continuous VS is applied to the problems of the continuous value function. The primary significance of the continuous VS is that it permits solely continuous functions to be solutions of fully nonlinear differential

equations, in which it provides general existence and uniqueness theorem [38]. The discontinuous VS has attracted attention with two motivations. The first motivation is that many optimal control problems may be discontinuous value functions. The second one is that VSs are considered stable with respect to certain relaxed semi-limits, which we call weak limits in the viscosity sense [39]. The weak limits are semi-continuous sub-solution or super-solution [40, 41].

In Crandall and Lions [37], the paper mainly focused on viscosity with continuous solutions. In control theory and the differential game theory, the applications of those theories do not have continuous solutions [42]. Especially in open channel flow, the discontinuities of water surface profiles are unavoidable phenomena. Thus, a deep understanding of discontinuous VSs of HJ equations is encouraged to study.

Other literature on discontinuous VSs has appeared in optimal control problems, differential game theory [43,44]. Also see several different notions of discontinuous solutions of HJ equations have been proposed in [45–50] to prove existence, comparison, and uniqueness results under various assumptions. In many cases, the difficulty of finding the analytical solution of uncertain differential equations yields proving an existence and uniqueness theorem of solution for differential equations under Lipschitz condition [50]. Ishii [52,53] was the first author to start systematically studying discontinuities both in the solutions and in the equations and his extension of "Perron's method" in the framework of VSs, which provides general existence results under very weak assumptions on the equations [43]. In Ishii's paper [52], the definition of possibly discontinuous viscosity sub- and super-solution is based on the concept of semi-continuous envelopes of the functions. The classical semi-continuous VSs were introduced. The Perron method was applied to show the existence

of possible classical semi-continuous solutions. The classical semi-continuous solutions are suitable for applications. The definition of classical semi-continuous solutions is a two-side notion with two differential inequalities. However, the uniqueness of such solutions remained uncertain since, in general, the classical comparison results for semi-continuous viscosity sub- and super-solutions do not imply the uniqueness of VSs. The essential limits to define semi-continuous envelopes were used instead in [53]. The use of the essential limits excluded some unnatural and artificial examples of admissible VSs (p.27 in [38]). Existence results of VSs were obtained from Lions [35]. The existence results for the classical first-order HJ equations have been proved in [54]. Barles and Perthame [45] were the first to introduce the stability and uniqueness of GSs with optimal control problems. Barron and Jensen stated that a paper by H.Frankowska [55] appeared, containing a related result. Her result is that a locally Lipschitz function is a VS of HJ equation with convex Hamiltonian if it is a GS in the sense of non-smooth analysis is a sub-solution in the stronger sense. Her proof does not apply to unbounded semi-continuous data [46].

Chapter 3

3 Application of level-set methods to the kinematic wave equation in open channel flows [56]

3.1 Introduction

Assessment of surface water flows is essential in understanding hydrodynamic phenomena such as flash floods, surge propagation, inundation resulting from dam breaks, tsunami, and flows resulting from the operation of hydraulic structures [57]. Those hydrodynamic phenomena influence humans, the environment, and economics [58]. For instance, the sudden release of water stored in a reservoir, namely dam breaks, could lead to severe environmental issues, risks to human life, and economic damage [59]. The more vulnerable areas at risk due to such flooding caused by dam breaks are the downstream dry bed terrains occupied by humans, infrastructures, industries, and agricultural lands. The

frequency of extreme precipitation events and floods is expected to increase due to global climate change [60]. Flood simulation outputs play pivotal roles in flood risk management [61]. Disaster risk reduction is better achieved if a socio-hydrological approach is well-linked with hydrodynamic modeling [62].

The surface water flows have been well comprehended in the context of the SWEs when the vertical scale is much smaller than the horizontal scale [9,27]. The 1D SWEs are hyperbolic systems that are routinely used to model the open channel system under the assumption of hydrostatic pressure [63–65]. The equation may induce the formation of hydraulic discontinuities, namely hydraulic jumps [30,66]. The SWEs have satisfactions in terms of simplicity and ease for physical interpretation [67]. Numerical solutions to the SWEs can reproduce the open system such as rivers, lakes, artificial channels, floodplains, and coastal areas [68], provided that errors resulting from truncation and round-off are appropriately managed as well as stability [69]. Up-to-date numerical schemes for SWEs can accurately approximate the solution to figure out the flow variables of the system in time and space [69–71]. They consist of two conservation laws: mass and momentum in analogy to the Navier-Stokes equations for incompressible fluids. The SWEs have been applied to various fields, such as coastal, environmental, and water resources engineering. Coastal engineering deals with tsunami wave propagation and tide currents. Liu et al. [72] compared linear and nonlinear SWEs describing tsunami-wave propagation over the China Sea. Zhu et al. [73] estimated tidal currents and residual currents using the SWEs to analyze their generation mechanisms. Akbar and Aliabadi [74] used hybrid finite element and finite volume techniques to solve two-dimensional (2D) SWEs for dealing with hurricane-induced storm surge flow problems. The SWEs have been consistently used in flood propagation,

flood inundation modeling, and river flooding in the field of water resources engineering and pollution transport problems in environmental engineering. Cozzolino et al. [75] considered simplifying the complete SWEs called the Local Inertia Approximation, which is derived by neglecting the advective term in the momentum equation. This model is generally applied to simulate slow flooding propagation at moving wetting-drying areas on even and uneven beds. A set of equations was derived from 1D SWEs to simulate 2D flood inundation [76]. Audusse and Bristeau [77] computed the transport of a passive pollutant with the SWEs using a finite volume kinetic method. Kuriqi and Ardıçlıoğlu [78] investigated the hydraulic regime of the Loire River in France using HEC-RAS, which is a widely adopted simulation software based on the 1D SWEs. Ardıçlıoğlu and Kuriqi [79] applied HEC-RAS to discuss the channel roughness of a natural river in six different flow regimes.

The complexity of the SWEs is attributed to the model dynamics of water with all aspects, including local acceleration term, convection acceleration term, pressure force term, gravity force term, and friction force term. There are two major approximations for the 1D SWEs. The first approximation method is diffusion wave approximation, in which the local acceleration term and convection acceleration term are not considered. The second one only considers the gravity force term and friction force term as force terms, resulting in the kinematic wave equation. The model is introduced initially and described explicitly in [17]. In the kinematic wave equation, several terms in the equation of motion, such as local acceleration term, convective acceleration term, and pressure force term, are assumed to be insignificant; hence, the equation of motion is simply expressed that the bed slope is equivalent to friction slope [80]. The kinematic wave equation has been employed in many hydraulic processes of subsurface flow, surface flow, sediment transport, solute transport,

and glacier hydrology. Singh [81] presented the history of the kinematic wave theory and its applications in water resources. Singh [5] discussed the general concept of the kinematic wave for overland flows, such as mathematical formulation and validity of the idea. The mixed runoff generation model and 2D kinematic wave model were introduced for overland flow routing in the upper Kongjiapo basin in the Qin River [82]. Huang et al. [83] combined rainfall-runoff and snowmelt modules derived from the kinematic wave equation and the energy budget method, respectively, to estimate the surface water resources in the semiarid area of Heilongjiang Province, China. Yomoto and Islam [84] used the kinematic wave equation for calculating the flood runoff discharge from the inclined upland field in Hiroshima Prefecture, Japan, concluding that the application of the kinematic wave equation with Manning's roughness produced better results than the other resistance law of Darcy and laminar.

In mathematical viewpoints, an initially dry bed for simulation of surface water flows using the kinematic wave equation is a challenging issue involving the deformation of the domain. Most conventional flow models assume sufficiently small positive water depths in the domain for a well-posed hyperbolic problem to avoid failure in producing solutions. The level-set method is robust in relaxing requirements for functional regularities of unknowns in nonlinear partial differential equations of the first order. The technique is one way to track the motion of propagating fronts or surfaces, which are considered zero level-set of higher level-set functions [85]. Initially introduced for curvature flows by Osher and Sethian [86], the overview of the level-set method to solve HJ equations has been described in the review paper by [87]. The technique has been seen in various fields such as image segmentation [88], computed tomography [89], and geometry optimization [90]. Li et al. [91] successfully

applied the level-set method to solving image segmentation, which faced intense inhomogeneity in real-world images. In structural engineering, the level-set method is used for structural optimization to minimize the structural load while satisfying the constraint [92]. Sethian and Smereka [93] tracked fluid interfaces. Duan et al. [94] proposed the variational level-set function to optimize the shape-topology in the Navier-Stokes problem by maintaining the smooth evolution without re-initialization and topology change. Yue et al. [95] presented a numerical method to simulate free-surface flows by solving the 3D incompressible Navier-Stokes equation with the level-set method. However, the kinematic wave equation has not yet been tackled with the level-set approach in the literature.

This study aims to clarify the advantages and limitations of the kinematic wave equation as the HJ equation. The level-set method is firstly applied to the continuity equation of 1D open channel flows, resulting in a nonlinear level-set equation of first order in a 2D space governing a level-set function whose zeros represent the water depths. Before analyzing surface water flows, the Eikonal equation is considered a primitive but vital example to comprehend the general idea of the level-set method. The Eikonal equation is often used to delineate the first-arrival time problems, and it has various practical applications, including computational geometry, computer vision, material science, etc. [11]. Transmit times for 3D seismic waves can be computed numerically from the Eikonal equation using the finite difference method [96]. However, the calculation of expanding wavefronts requires the notion of characteristics [97]. Therefore, we numerically compute the level-set function for the kinematic wave equation with a characteristic method. The numerical solutions are verified with the analytical solutions of relevant dam-break problems. The weak analytical solutions

of the dam-break problems are obtained from theoretical celerity, which becomes the speed of propagating shock front on a dry bed. However, it turns out that the issues related to overturning phenomena appear. In order to control the development of overturning, singular viscosity regularization (SVR) is employed [98]. Then, the computational results with and without SVR are compared with the weak analytical solution representing the time evolution of the shock front propagating downstream, optimizing a parameter of SVR. Finally, the study of abrupt water release from Chan Thnal Reservoir, Kampong Speu Province, Cambodia, into its irrigation canal system with the initially dry bed is simulated as a practical demonstrative example.

3.2 Methodology

Mathematical models for surface water flows involve nonlinear partial differential equations. In this section, the kinematic wave equation is derived from the SWEs, and the level-set method is briefed with the Eikonal equation. The kinematic wave equation and the Eikonal equation are regarded as HJ equation. In the larger type of equation, both equations and SWEs are the first-order quasilinear differential equations. The kinematic wave equation is solved by the level-set method with the assistance of SVR. Inclusion relations and dependency among those concepts are delineated in **Figure 3.1**.

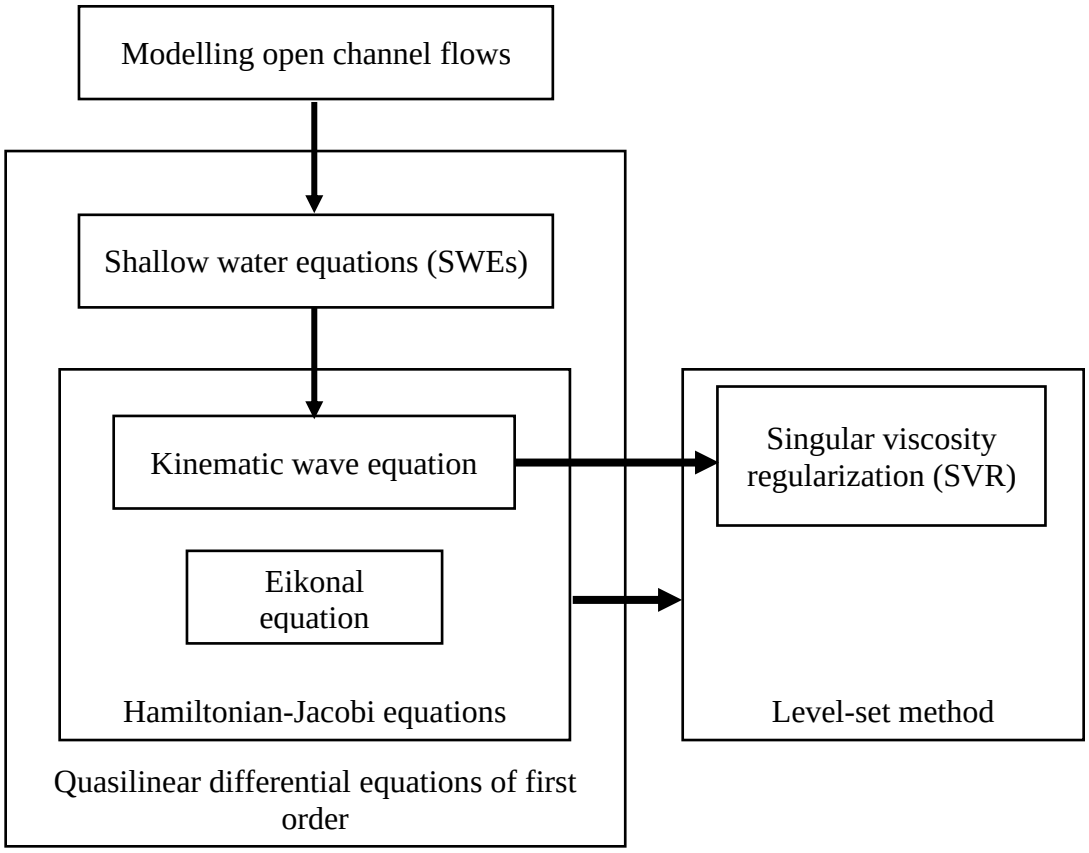

Figure 3.1. Inclusion relations and dependency among the concepts in the methods.

3.2.1 Governing equation of open channel flows

The SWEs consist of the continuity equation and momentum equation, representing the laws of mass conservation and momentum conservation, respectively. In 1D surface water flows of hydrostatic pressure distribution, the SWEs are written as

$$\frac{\partial}{\partial t}\begin{pmatrix} A \\ Q \end{pmatrix} + \frac{\partial}{\partial x}\begin{pmatrix} Q \\ \dfrac{\beta Q^2}{A} \end{pmatrix} = \begin{pmatrix} q \\ -gA\dfrac{\partial \eta}{\partial x} - gAS_f \end{pmatrix} \tag{3.1}$$

where t is the time (s), $A = A(x,z)$ is the cross-sectional area (m^2), Q is the discharge (m^3/s), x is the local curvilinear abscissa along the channel bed (m), β is the momentum coefficient, η is the water level (m), q is the lateral inflow discharge per unit length (m^2/s), g is the acceleration due to gravity (m/s^2), and S_f is the friction slope which is given by the Manning's formula

$$S_f = \frac{n^2 Q|Q|}{A^2 R^{4/3}} \tag{3.2}$$

where n is Manning's roughness coefficient, and R is the hydraulic radius (m).

3.2.2 Kinematic wave approximation

There are approximation techniques for the SWEs. The momentum equation of (**3.1**) is approximated in these approximation techniques, while the continuity equation of (**3.1**) remains in the original form. Considering the term $gA\dfrac{\partial \eta}{\partial x}$ in the momentum equation can be divided into two terms as

$$-gA\frac{\partial \eta}{\partial x} = -gA\frac{\partial Z_b}{\partial x} - gA\frac{\partial h}{\partial x} = gAS_0 - \frac{\partial}{\partial x}\left(g\int_0^h \frac{\partial A}{\partial z}(h-z)\,dz \right), \tag{3.3}$$

where h is the water depth (m), Z_b is the bed elevation (m), z is the upward vertical axis (m), and S_0 is the bed slope.

The momentum equation can be understood in the conservative form as

$$\frac{\partial Q}{\partial t}+\frac{\partial}{\partial x}\left(\frac{\beta Q^2}{A}+g\int_0^h\frac{\partial A}{\partial z}(h-z)\,dz\right)=gAS_0-gAS_f \tag{3.4}$$

(a) (b) (c) (d) (e)

where each term denotes (a) the local acceleration, (b) the convection acceleration, (c) the pressure, (d) the gravity, and (e) the friction terms. The kinematic wave approximation consists only of the gravity and friction terms. The diffusion wave approximation considers the pressure, gravity, and friction terms. The non-inertia wave approximation is based on the local acceleration term in addition to the diffusion wave approximation. The gravity wave approximation includes the local acceleration, the convective acceleration, and the pressure terms. The quasi-steady dynamic wave equation employs all the terms of SWEs except the local acceleration term. The original form of SWEs is referred to as dynamic wave approximation.

The kinematic wave approximations are generally applied to open channel flow simulations in rivers, canal systems, or overland flow resulting in less theoretical and computational complexity. The kinematic wave approximation assumes local equilibrium of momentum, negligible pressure gradient, and $S_0=S_f$, to reduce **(3.1)** to

$$\begin{cases}\dfrac{\partial A}{\partial t}+\dfrac{\partial(AV)}{\partial x}=q\\ V=\dfrac{1}{n}R^{2/3}S_0^{1/2}\end{cases} \tag{3.5}$$

where V is the cross-sectional averaged velocity (m/s). When a dry bed takes place, the cross-sectional averaged velocity V simply vanishes.

3.2.3 Analytical solution of the kinematic wave equation

Analysis of the kinematic wave equation stems from regarding the system **(3.5)** as a quasilinear differential equation of first order expressed as

$$\frac{\partial u}{\partial t}+\frac{\partial F(u)}{\partial x}=r \tag{3.6}$$

where u is a generic unknown variable, F is the flux which is a nonlinear function of u, and r is a source term. For a piecewise continuous GS having a jump from u_l to u_r, the local celerity is given by

$$C(u_l,u_r)=\frac{F(u_l)-F(u_r)}{u_l-u_r} \tag{3.7}$$

provided that $F'(u_l)>C(u_l,u_r)>F'(u_r)$ [99]. In the continuous case, the celerity approaches to

$$C(u,u)=\frac{\partial F(u)}{\partial u}, \tag{3.8}$$

which is known as the Kleitz-Seddon law in the context of the kinematic wave equation. The analytical solutions will be employed to verify the level-set method with SVR appropriately working.

3.2.4 Level-set method

The level-set method firmly relies on the HJ equation, which often appears in variational calculus. The conservative form **(3.6)** is formally rewritten as the HJ equation **(3.9)**

$$\frac{\partial u}{\partial t} + H\left(t, x, u, u_x\right) = 0 \tag{3.9}$$

where H is the Hamiltonian. The notion of VS is commonly applied to HJ equations. The level-set function $\phi = \phi(t, x, z)$ is a function of *t*, *x*, and another secondary independent variable *z*, such that its zeros represent *u* $\left(\phi(t, x, u) = 0\right)$. The governing equation of ϕ is the level-set equation

$$\frac{\partial \phi}{\partial t} - \frac{\partial \phi}{\partial z} H\left(t, x, z, -\frac{\phi_x}{\phi_z}\right) = 0 \tag{3.10}$$

which must be treated in the viscosity sense, as it is formally derived from $\phi_t + \phi_z u_t = 0$ and $\phi_x + \phi_z u_x = 0$ [98].

3.2.5 Example of the level-set method applied to Eikonal equation

A primitive but essential application of the level-set method is to the Eikonal equation. The unsteady form of the Eikonal equation is

$$\frac{\partial u}{\partial t} + \left|\frac{\partial u}{\partial x}\right| = 1 \tag{3.11}$$

whose Hamiltonian H is

$$H\left(t, x, u, p_1\right) = H\left(p_1\right) = \left|p_1\right| - 1 \tag{3.12}$$

where p_1 is u_x as an argument of Hamiltonian and the corresponding level-set equation is

$$\frac{\partial \phi}{\partial t} - \frac{\phi_z}{|\phi_z|}\left|\frac{\partial \phi}{\partial x}\right| + \frac{\partial \phi}{\partial z} = 0\,. \tag{3.13}$$

The level-set function **(3.13)** with the initial and boundary condition $\phi(0, x, z) = z$ and $\phi(t, \pm 1, z) = z$ is numerically computed in the *t*-*x*-*z*-domain $(0,6)\times(-1,1)\times(-2,2)$, using an upwind differencing discretization scheme in the *x*-*z*-space and the fourth-order Runge-Kutta method in time *t*. With meshes of $\Delta t = 0.1$, $\Delta x = 0.1$, and $\Delta z = 0.1$, the computed results at $t =$ 0, 1, 2, and 3 are presented in **Figure 3.2**, where the zeros are highlighted with different colors for different times. As the solution *u* to the Eikonal equation **(3.11)** represents the minimum first exit time from the domain, there is a steady-state

$$u = 1 - |x|, \tag{3.14}$$

which is achieved within a finite time. The computational results well reproduce the solution, as can be seen from the transient state at *t* = 1 followed by the identical values at *t* = 2 and 3. However, the case of the kinematic wave equation is not straightforward due to the vanishing Hamiltonian for dry beds.

3.2.6 *Derivation of level-set equation for the kinematic wave equation*

For the sake of simplicity, the unit width of an open channel having a very broad rectangular cross-section without any lateral flow is considered in the kinematic wave equation **(3.5)**, implying that $R = h$, $u = h$, $F(u) = \left(S_0^{1/2}/n\right)u^{5/3}$, and $F'(u) = \left(5S_0^{1/2}/3n\right)u^{2/3}$, where *h* is the water depth.

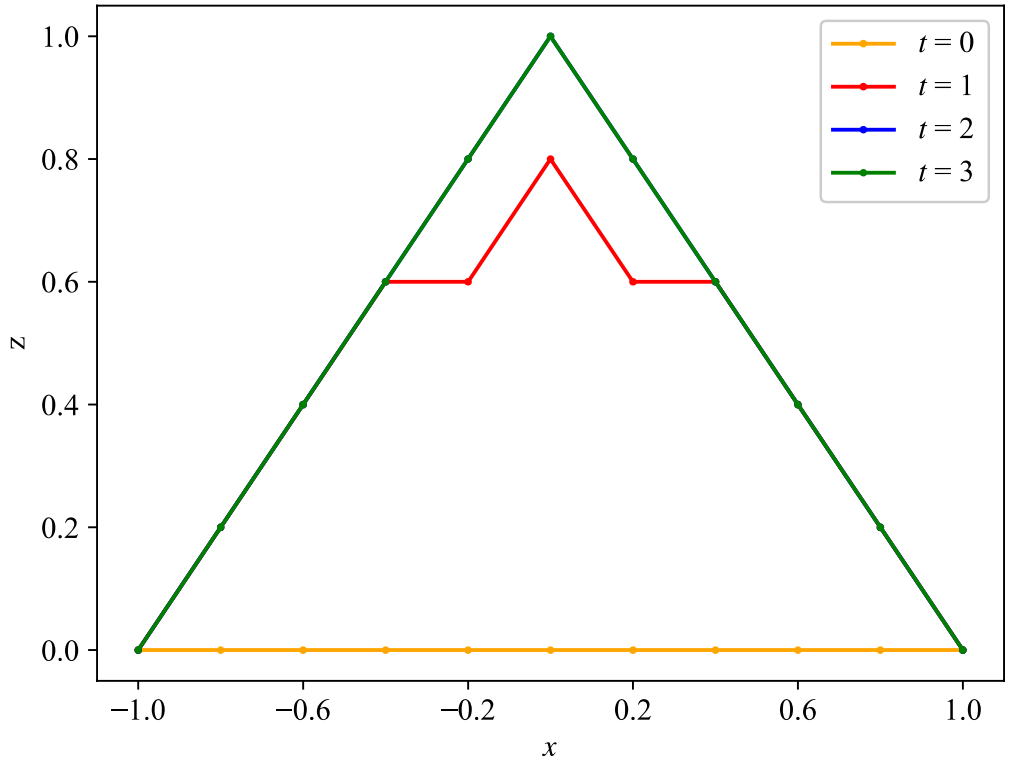

Figure 3.2. Numerical solutions to the level-set equation for the Eikonal equation.

The bed slope S_0 and the Manning's roughness n are assumed piecewise constant. Then, the Hamiltonian H becomes

$$H\left(t,x,u,p_1\right)=\frac{5S_0^{1/2}}{3n}u^{2/3}p_1 \tag{3.15}$$

and then the level-set equation becomes

$$\frac{\partial\phi}{\partial t}+\frac{5S_0^{1/2}}{3n}z^{2/3}\frac{\partial\phi}{\partial x}=0 \tag{3.16}$$

which governs ϕ almost everywhere in the t-x-z-domain $\left(0,\infty\right)^3$. The initial condition is imposed as

$$\phi(0, x, z) = z \tag{3.17}$$

to represent the initial dry bed. Then, assuming dam-break or sudden operation of a hydraulic structure at the upstream end, the boundary condition

$$\phi(t, 0, z) = z - h^{\text{up}} \tag{3.18}$$

is imposed to specify the upstream water depth as h^{up}. Although u is a function of bounded variation (BV function) allowing discontinuities, the level-set function ϕ is possibly continuous in the domain but not up to the boundary. Since there is no term of ϕ_z, **(3.16)** is solved as an advection equation in the *t*-*x*-domain $(0, \infty)^2$.

3.2.7 *The computational method with SVR*

The domain is discretized into meshes of equal size Δt by Δx by Δz, to compute the approximate values of ϕ. The notation $\phi_{k,i,j}$ represents the approximated $\phi(k\Delta t, i\Delta x, j\Delta z)$ for $k, i, j \in \mathbb{Z}$. The characteristic method analogous to solving a Bellman equation in dynamic programming is employed [100]. The piecewise linear interpolation is applied to the *x*-direction as

$$\hat{\phi}(k\Delta t, x, j\Delta z) = \phi_{k,i,j} + (\phi_{k,i+1,j} - \phi_{k,i,j}) \frac{x - i\Delta x}{\Delta x} \tag{3.19}$$

where $\hat{\phi}$ is the interpolated ϕ, and $i\Delta x \le x < (i+1)\Delta x$. Then, the level-set equation **(3.16)** is approximately solved as

$$\phi_{k+1,i,j} = \hat{\phi}\left(k\Delta t, \xi, j\Delta z\right) = \phi_{k,i,j} + \left(\phi_{k,i+1,j} - \phi_{k,i,j}\right)\frac{\xi - i\Delta x}{\Delta x} \tag{3.20}$$

where

$$\xi = i\Delta x - \frac{5S_0^{1/2}}{3n}\left(j\Delta z\right)^{2/3}\Delta t\,. \tag{3.21}$$

Overturning happens when the upper part of a solution moves faster than the lower part [98]. In a practical implementation of **(3.20)**, the overturning may develop due to violation of the minimum principle $\phi_z\left(t,x,z\right) \geq 0$ for $t \geq 0$, and adding a singular viscosity term ψ to **(3.16)** serves as regularization. The level-set equation with SVR is

$$\frac{\partial\phi}{\partial t} + \frac{5S_0^{1/2}}{3n}z^{2/3}\frac{\partial\phi}{\partial x} = \psi\,. \tag{3.22}$$

The singular viscosity term $\psi_{k,i,j}$ at the discretized stage is given as

$$\psi_{k,i,j} = M\left|\left(\nabla\phi\right)_{k,i,j}\right|\frac{\tanh\left(\gamma\dfrac{\phi_{k,i,j+1}-\phi_{k,i,j}}{\Delta z}\right) - \tanh\left(\gamma\dfrac{\phi_{k,i,j}-\phi_{k,i,j-1}}{\Delta z}\right)}{\Delta z} \tag{3.23}$$

where

$$\left|\left(\nabla\phi\right)_{k,i,j}\right| = \sqrt{\left(\frac{\phi_{k,i+1,j}-\phi_{k,i-1,j}}{2\Delta x}\right)^2 + \left(\frac{\phi_{k,i,j+1}-\phi_{k,i,j-1}}{2\Delta z}\right)^2} \tag{3.24}$$

with parameters M to be optimized and $\gamma = 1/\Delta z$, as recommended in the paper [98].

The zeros of the computed level-set function at each time stage $k\Delta t$, which are represented by $\left(\xi_{k,i,j}, j\Delta z\right)$ or $\left(i\Delta x, \zeta_{k,i,j}\right)$, solve

$$\phi_{k,i,j} + \left(\phi_{k,i+1,j} - \phi_{k,i,j}\right)\frac{\xi_{k,i,j} - i\Delta x}{\Delta x} = 0 \tag{3.25}$$

with $i\Delta x \le \xi_{k,i,j} < (i+1)\Delta x$ or

$$\phi_{k,i,j} + \left(\phi_{k,i,j+1} - \phi_{k,i,j}\right)\frac{\zeta_{k,i,j} - j\Delta z}{\Delta z} = 0 \tag{3.26}$$

with $j\Delta z \le \zeta_{k,i,j} < (j+1)\Delta z$, respectively, for each i and j.

3.3 Results

3.3.1 *Dam-break problems with and without SVR*

The level-set method for the kinematic wave equation is now applied to the dam-break problems with the dry bed initial condition. Without loss of generality, $S_0^{1/2}/n = 1$ is assumed, and the local celerity of dam-break flows over the dry bed becomes $C(u,0) = u^{2/3}$ (m/s) in the model. Numerical experiments for the level-set equation are performed over the subset $(0,100]\times(0,500]\times(0,12)$ of $(0,\infty)^3$, with meshes of $\Delta t = 0.01$ (s), $\Delta x = 1$ (m), and $\Delta z = 0.5$ (m). The boundary $x = 0$ is considered as the position of a dam, separating upstream and downstream areas. At the initial time, the downstream site is set to be a dry bed. Setting a boundary condition to specify a water depth h^{up} at $x = 0$ formulates a dam-break problem for the kinematic wave equation. Firstly, the dam-break problem for h^{up} = 2 (m) is numerically solved by the level-set method without SVR. **Figure 3.3** compares the computed zeros of the level-set function (circular dots, noSVR) with the exact positions of

the shock fronts obtained from the analytical solution (dash lines, Exact). The different colors show the time stages every 10 (s) as the shock front propagates downstream. The computed zeros constitute the upstream water surface $h^{up} = 2$ (m) and the propagating shock front for each *t*. However, the overturning phenomena occur, which cause unwanted shock front motion. Hence, SVR is introduced with an optimized $M = 0.01$ in **Table 3.1**. The results are similarly depicted in **Figure 3.4** where the triangular dots indicate the zeros of level-set function with SVR (SVR). The overturning remains in the zeros of level-set function with SVR; however, they better approximate the analytical solution with reasonable reproduction of celerity.

The results of upstream water surface 5 and 10 (m) are shown in **Figure 3.5** and **Figure 3.6**, respectively. Similar results and interpretations like upstream water surface $h^{up} = 2$ (m) can be applied to different cases of upstream water surface 1-10 (m) with different values optimized M in **Table 3.1**.

Table 3.1. The optimal coefficient *M* for upstream water depth from 1-10 (m).

h^{up} (m)	*M*
1	0.0001
2	0.01
3	0.04
4	0.05
5	0.08
6	0.15
7	0.25
8	0.3
9	0.4
10	0.5

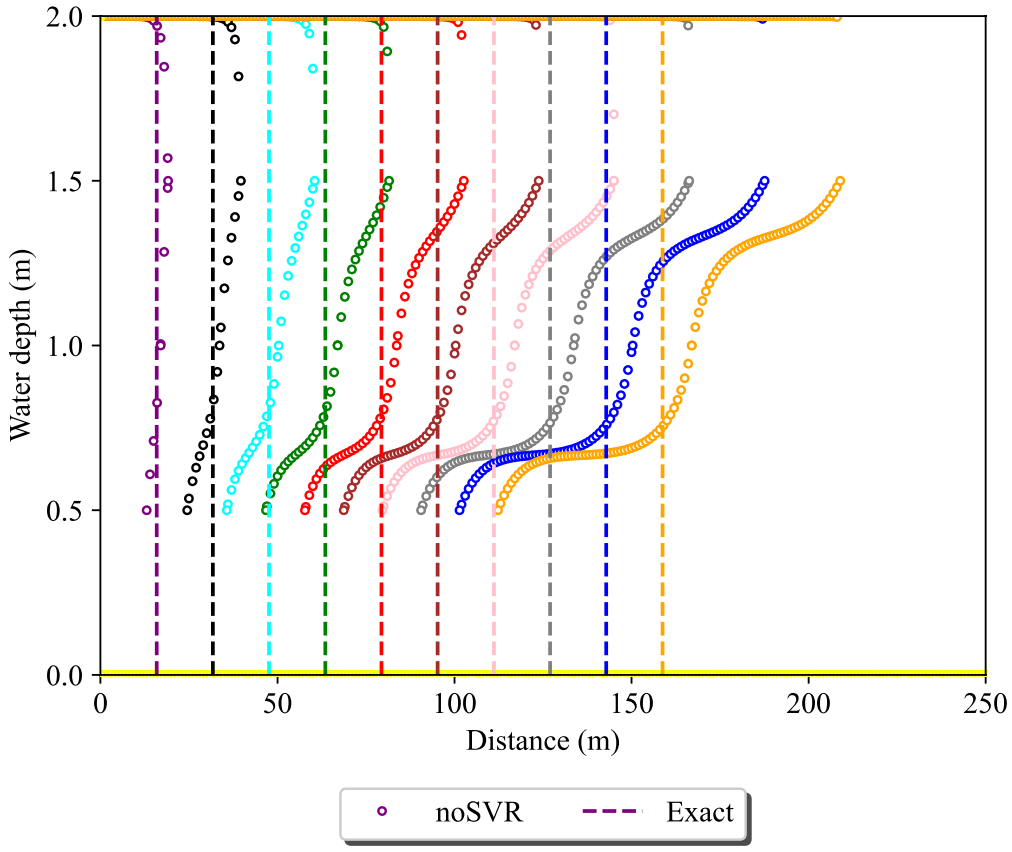

Figure 3.3. Zeros of the computed level-set function without SVR (noSVR) for the dam-break problems over the dry bed in comparison with the exact positions of the shock front (Exact) for the case h^{up}=2 (m). The different colors show the time stages every 10 (s) for total computation period of 100 (s).

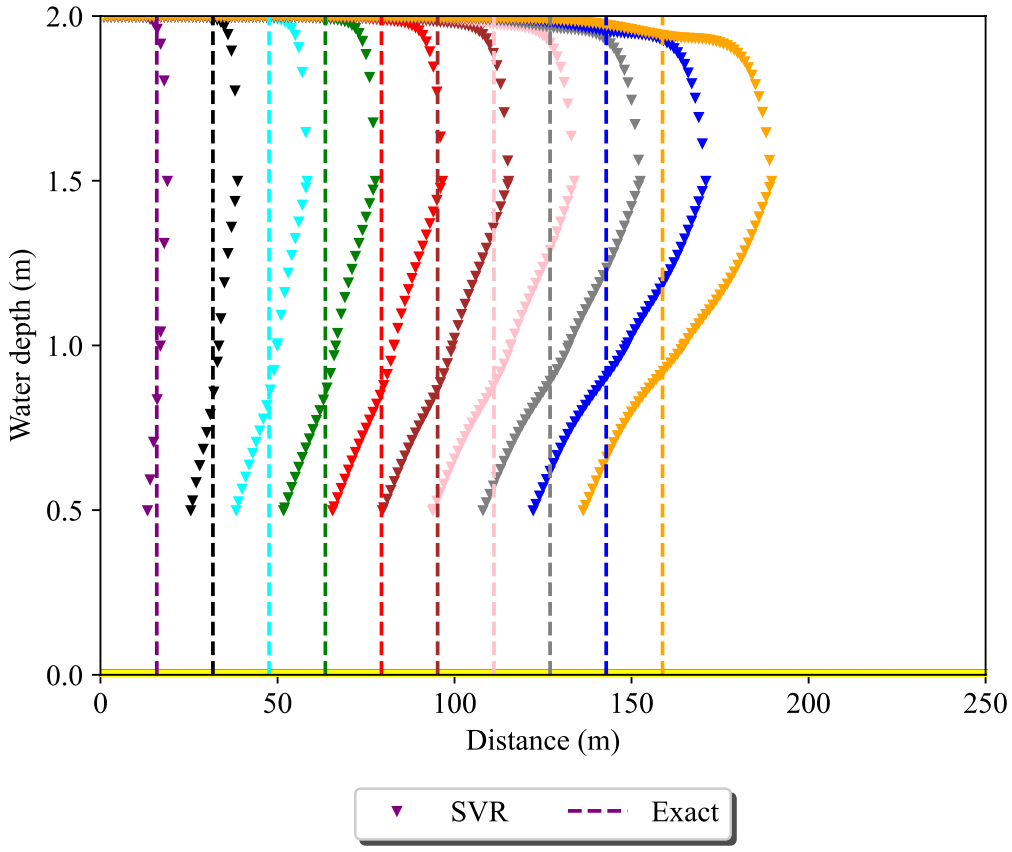

Figure 3.4. Zeros of the computed level-set function with SVR (SVR) for the dam-break problems over the dry bed in comparison with the exact positions of the shock front (Exact) for the case h^{up}=2 (m). The different colors show the time stages every 10 (s) for total computation period of 100 (s).

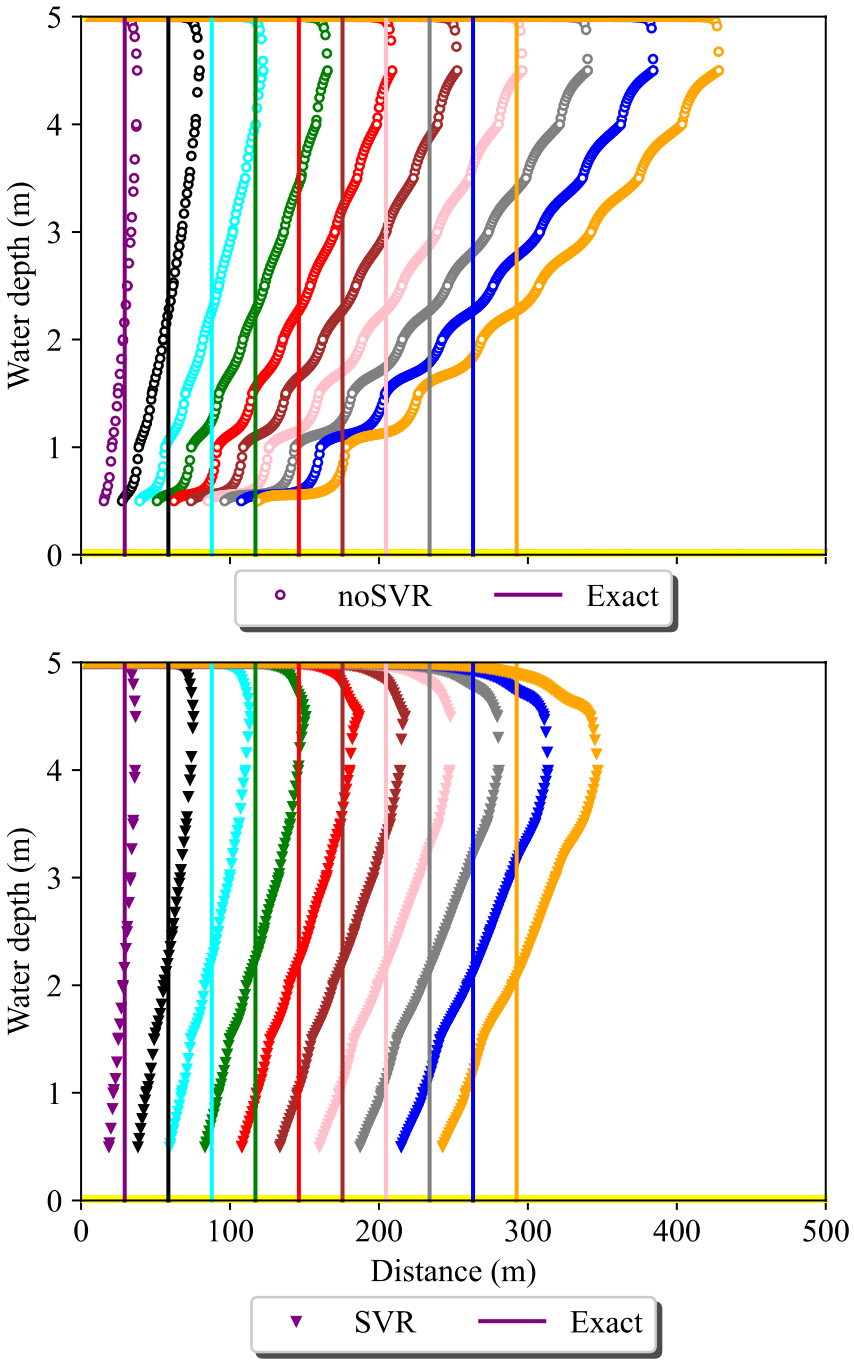

Figure 3.5. Zeros of the computed level-set function without SVR (upper) and with SVR (lower) for the dam-break problems over the dry bed in comparison with the exact positions of the shock front (Exact) for the case h^{up}=5 (m).

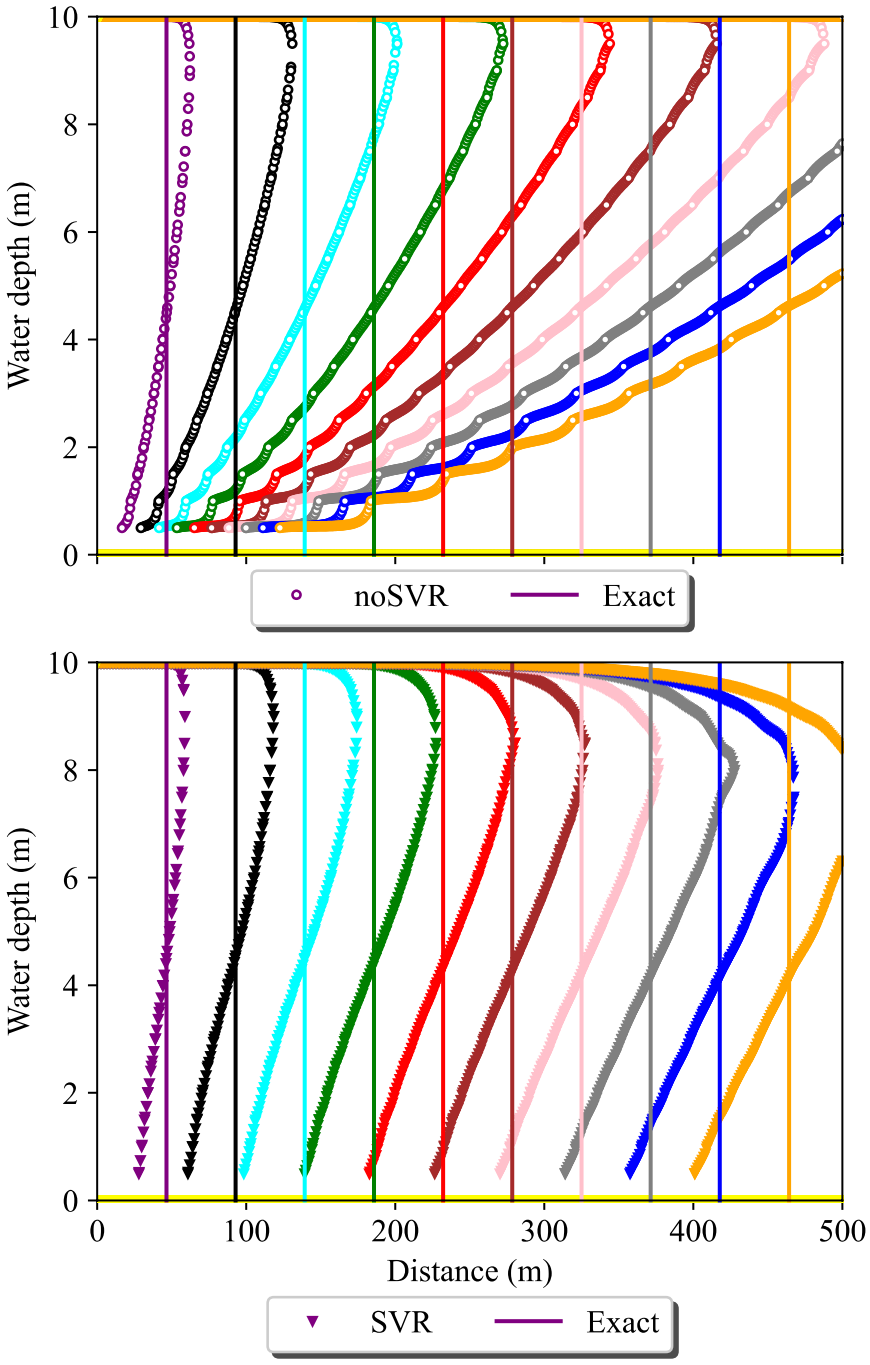

Figure 3.6. Zeros of the computed level-set function without SVR (upper) and with SVR (lower) for the dam-break problems over the dry bed in comparison with the exact positions of the shock front (Exact) for the case h^{up}=10 (m).

3.3.2 *Optimal values of coefficient M*

Coefficient *M* and γ are two parameters required to be specified when SVR is included in the level-set method. According to Tsai *et al*. [98], γ was set to be $1/\Delta z$; however, *M* was stated to be a sufficiently large value. In such a case, the coefficient *M* has not well defined in the paper. Thus, this study examines the optimal values of the coefficient *M* by implementing different cases of boundary conditions: h^{up} = 1, 2,…, 10. The subset and meshes where numerical experiments are performed are the same as in subsection 3.3.1. For each case of h^{up}, different values of *M* in the range $(0,1)$ are specified to produce the corresponding zeros of the level-set function with SVR. For each value of *M*, the minimum distance between the zeros of the level-set function and the exact solution is calculated to obtain the optimal value of the coefficient *M*. The optimized results of the coefficient *M* for the different cases of h^{up} from 1-10 (m) are summarized in **Table 3.1** and **Figure 3.7**. The higher upstream water depth is, the greater the coefficient *M* is needed. The relation is approximated by the quadratic function of $M = 0.0063h^{up2} - 0.0134h^{up} + 0.0098$ with $R^2 = 0.99$.

To visualize the difference between the cases with and without the optimized SVR, the error in each case is determined by the maximum distance between the zeros of the level-set function and the exact positions of shock fronts, as illustrated in **Figure 3.8**. The green dots and the red dots represent the errors in the cases without and with the optimized SVR, respectively. **Figure 3.8** implicates that the effect of SVR is so significant that it bounds the error without depending on h^{up}.

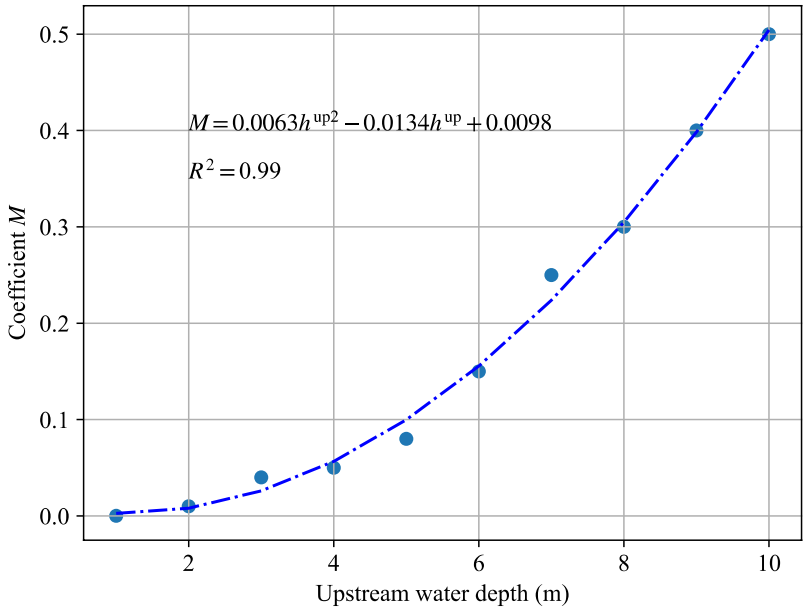

Figure 3.7. The optimal coefficient *M* for different cases of upstream water depth from 1-10 (m).

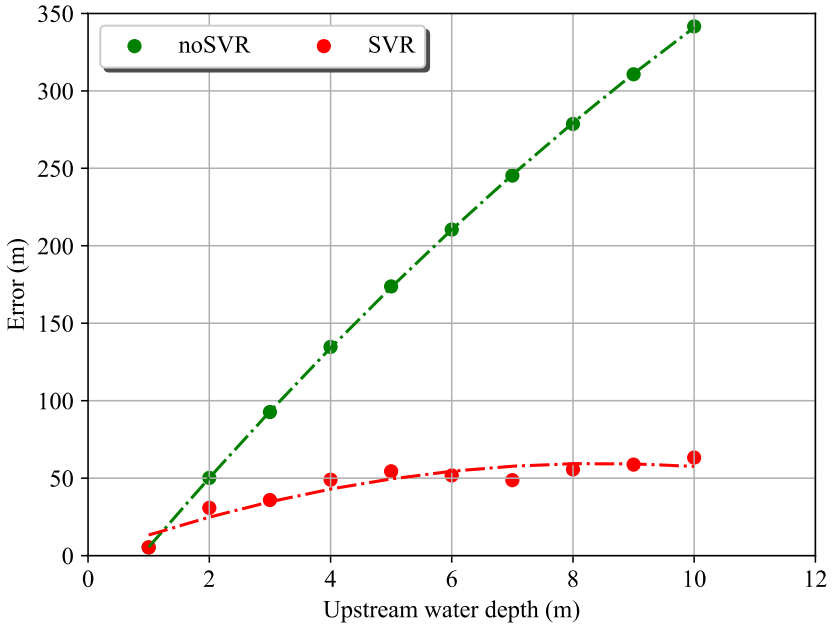

Figure 3.8. The errors in the zeros of the level-set functions without SVR (green dots) and with the optimized SVR (red dots).

3.3.3 *A practical demonstrative example of Chan Thnal Reservoir to an irrigational canal system*

Chan Thnal Reservoir is located in Kampong Speu Province of Cambodia, having a maximum capacity of 3 million cubic meters. It collects rainwater from a catchment area of 268 km^2, supplying the stored water to the irrigation canal system from the main gate at the coordinates 11°34'13"N and 104°31'26"E [101]. As one of the central lowlands of Cambodia, the average annual rainfall in Kampong Speu Province is about 1400 mm [102]. Tropical Monsoon climate usually shows the characters of a unimodal rainfall intensity curve with a specific long dry spell [103], and the catchment area and the command area of Chan Thnal Reservoir are not an exception. The reservoir is operated both in the rainy seasons (May to October) for 1000 ha of the agricultural zone and in the dry seasons (November to April) for 115 ha, often encountering the problem of abrupt water release to an initially dry bed of the irrigation canal system. Such operation may aim to increase water efficiency in agriculture and enhance the flood retention function of the reservoir [104]. The map of Cambodia, Kampong Speu Province, and the study site of Chan Thnal Reservoir and the irrigation canal are shown in **Figure 3.9**. The main canal of the system, having a total length of 7320 m is modeled as an open channel with varied bed slopes, which are approximately 1/112, 1/547, 1/628, 1/499, and 1/2079 for the five reaches divided by the points 610 m, 2070 m, 3670 m, and 5060 m distant from the reservoir. A constant Manning's roughness $n = 0.03$ ($m^{-1/3}s$) is applied to the model since the canal is an earthen type with vegetation [31].

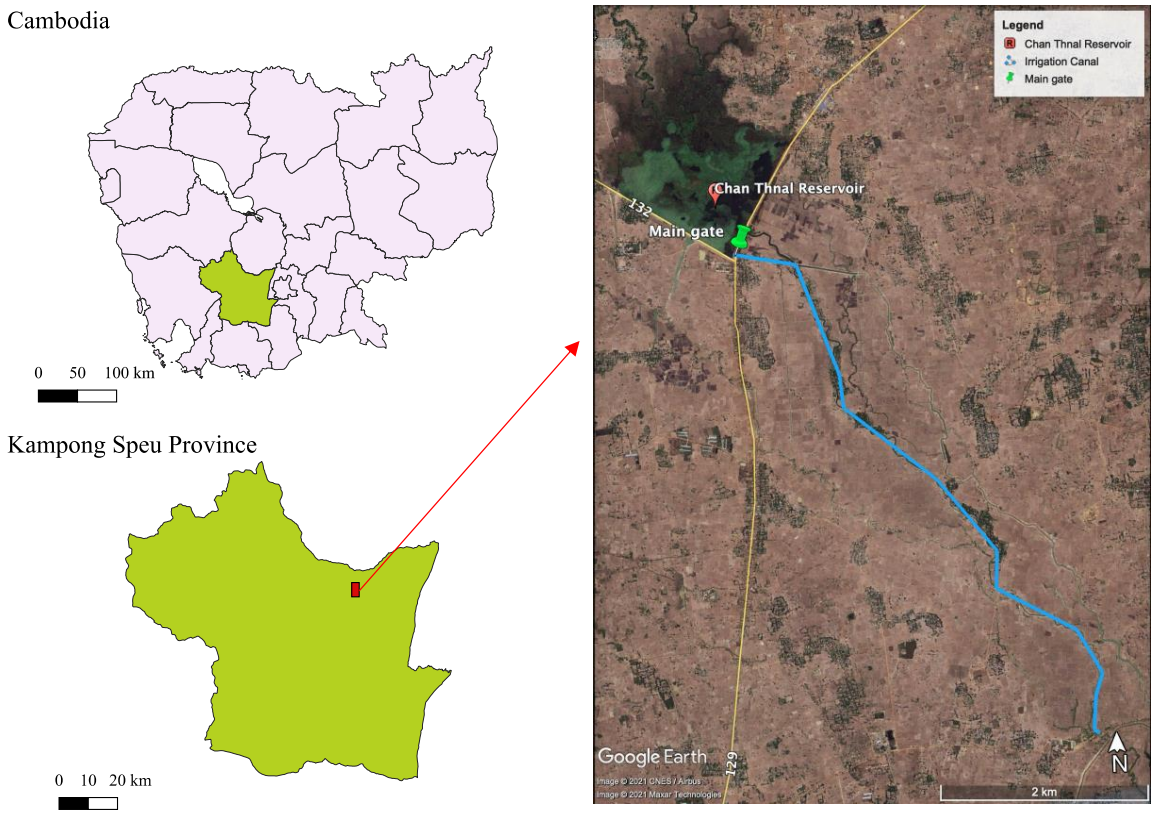

Figure 3.9. Map of Cambodia, Kampong Speu Province, and satellite image of Chan Thnal Reservoir and its irrigational canal (blue line) (Google Earth image taken on January 12th, 2014, accessed on June 02nd, 2021).

The ability of the level-set method with SVR applied to the kinematic wave equation is demonstrated in the practical problem of abrupt water release from Chan Thnal Reservoir into an initially dry bed of the main canal. The level-set equation is numerically solved for the dam-break problem for $h^{up} = 2$ over the subset $(0,3600]\times(0,7320]\times(-1,3)$ of $(0,\infty)^3$, with meshes of $\Delta t = 0.1$ (s), $\Delta x = 10$ (m), and $\Delta z = 0.1$, considering the varied bed slopes. As we have observed in the primitive test cases, strong overturning occurs as the fronts propagate downstream when M is small. If M is large, then artificial diffusion takes place

so that the upper parts of the fronts tend to move slower than the lower parts. With an optimized value of $M = 0.003$, surface water flows are computed and delineated in **Figure 3.10**. The computed zeros of the level-set function are plotted every 100 (s) with different colors for the computational period of 3600 (s). It is seen that the fronts propagate downstream; however, the surface water flows do not change with the bed slopes.

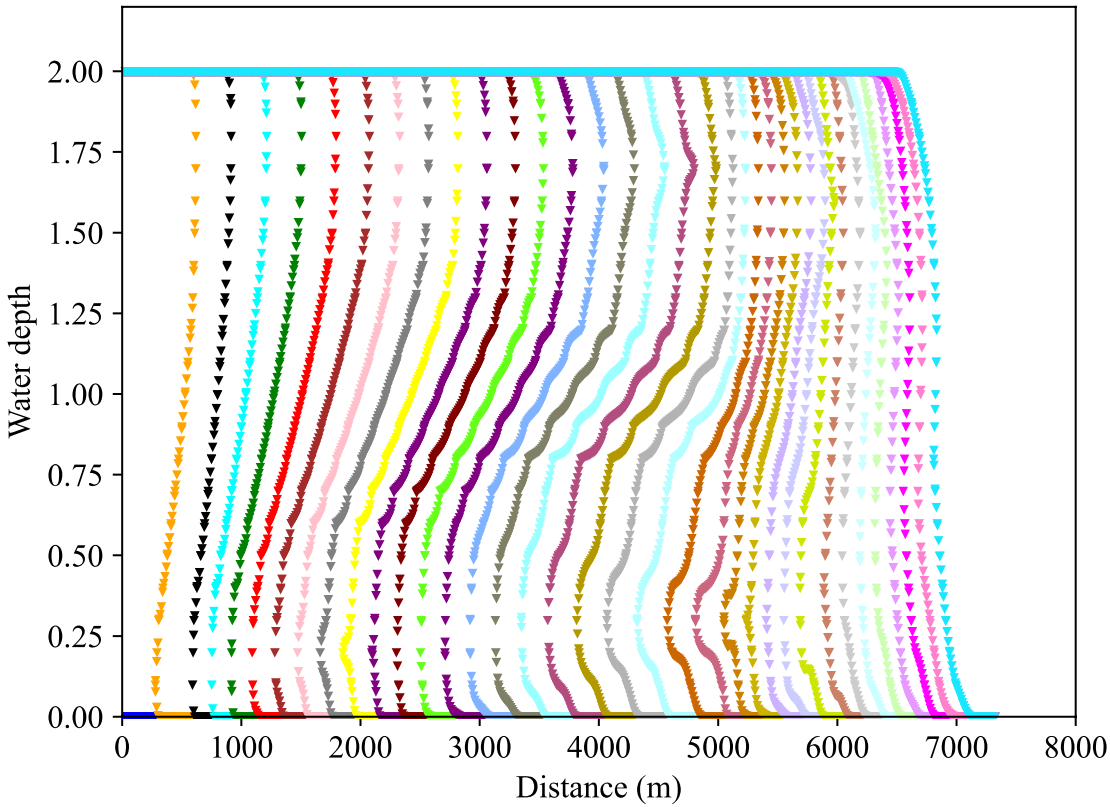

Figure 3.10. Zeros of the computed level-set function with SVR over the dry bed of irrigation canal of Chan Thnal Reservoir for $h^{up}=2$. The different colors show the time stages every 100 (s) for total computation period of 3600 (s).

3.4 Discussion

The standpoint regarding the kinematic wave equation as the HJ equation has been almost untracked. Still, the model development and the numerical experiments conducted here have revealed their advantages and limitations.

The kinematic wave equation remains hyperbolic even if the water depth becomes zero and does not involve any well-posedness issue when dealing with the initially dry bed problems. At the same time, the dam-break problems imply discontinuities in the water depths. The level-set method is powerful in relaxing requirements for functional regularities of unknowns in nonlinear partial differential equations of the first order, including HJ equations. Inhomogeneous slight overturning phenomena can be seen in the propagating shock front, mainly in the midstream of the irrigation canal, implicating that the constant coefficient M was not optimal. The Froude numbers achieved after the arrival of the shock front were 1.1272, 0.5069, 0.4779, 0.5343, and 0.2672 for the five reaches divided by the points 610 m, 2070 m, 3670 m, and 5060 m distant from Chan Thnal Reservoir, respectively, implying that there was a hydraulic jump in terms of the SWEs at the point 610 m from the reservoir. This incapability of detecting hydraulic jumps is one of the limitations of the level-set method for the kinematic wave equation. While, in contrast to most of the available software tools using either the 1-D SWEs with some artificial viscosity or the diffusion wave approximation, the method results to be free from spurious diffusive deformation of water surfaces. As demonstrated in the practical example with $\Delta x = 10$ (m) and $\Delta z = 0.1$, the use of relatively coarse mesh admits the method's efficiency despite the fact that the computation

is implemented in the 2-D space. When the bed slopes vary, the surface water flows remain constant at 2. This may possibly result from the assumption of $S_0^{1/2}/n = 1$. Thus, the computational method does not work successfully in the practical demonstrative example of the Chan Thnal irrigation canal with varied bed slopes. Another treatment is needed for the case.

The critical point of applying the level-set method to the kinematic wave equation is the requirement of SVR. The applications of the level-set method to the kinematic wave equation with and without SVR have been compared and verified with analytical solutions of dam-break problems. These results clearly indicated the importance of SVR in improving the numerical solutions.

3.5 Conclusions

This chapter discussed the applicability of the level-set method to the kinematic wave equation for the reproduction of propagating discontinuous water surface caused by dam-break over an initially dry bed on the downstream side. Unlike the Eikonal equation, overturning is intrinsic to the kinematic wave equation whose Hamiltonian vanishes on the dry bed. The introduction of SVR was effective for relocating the zeros of the level-set function close to the correct positions of the shock front. However, that effect was sensitive to the coefficient *M*, which was optimized to produce a better numerical solution of the level-set function for each case of upstream water depth. The relation between upstream water depth and coefficient *M* is approximated by the quadratic function of $M = 0.0063h^{\mathrm{up}2} - 0.0134h^{\mathrm{up}} + 0.0098$ with

$R^2 = 0.99$. The maximum distance between the zeros of the level-set function and the exact positions of shock fronts was used for determining the error. An essential outcome of this study is to implicate that SVR can uniformly suppress the overturning phenomena, which might linearly grow as the upstream water depth is increased. Finally, the practical application understandably shows that the level-set method with SVR applied to the kinematic wave equation is versatile for dry beds. However, its application over the varied bed slopes has not successfully tackled.

The level-set method for the full SWEs over standard digital elevation mesh shall be tackled in the follow-up study to develop methodologies for better understanding the practical hydrodynamic phenomena. Future works shall also deal with technical issues such as the treatment of the irregular channel topography, roughness, lateral flows, and then channel junctions.

Chapter 4

4 Numerical demonstrations of non-dissipative discontinuous kinematic waves in open channel flows

4.1 Introduction

The governing equations of one-dimensional (1D) open channel flows include the local acceleration term, the convective acceleration term, the pressure term, the gravity force term, and the friction force term, constituting a complicated nonlinear hyperbolic system. Lighthill and Whitham [17] originally introduced the kinematic wave model under the assumption of balanced gravity and friction forces. It has been widely applied in open channel hydraulics and surface hydrology for a long time.

Astonishingly, there persists a misunderstanding among engineers regarding the kinematic wave model's fundamental properties, as shown in the recent review paper of

Singh [5], stating as follows. “Shock is defined as a discontinuity in the continuum of flow and is transient. In other words, it develops and dissipates. A shock can occur where there is a sudden step rise in rainfall intensity, a sudden change in bed roughness, bed elevation, etc. An analogy with traffic flow is instructive in that traffic jam, which is analogous to a shock, occurs where there is a reduction of lanes on the highway, stop sign, traffic light, accident, but over time it dissipates”.

This study clarifies that a discontinuity can develop without dissipation even under the smoothness of all input in the kinematic wave model. This phenomenon reflects physical processes such as hydraulic jumps and surges. The propagation of discontinuities, which occurs even from smooth initial data, has been stated in the papers [30,105–109]. Such a phenomenon is intrinsic to FOQL PDEs, including the kinematic wave model, the Kynch’s sedimentation model [110], the compressible Euler equations [111], and the traffic flow models [112–114]. Jin *et al*. [113] proposed a model of the capacity drop occurring at an operational bottleneck in the framework of the kinematic wave model. The capacity-drop phenomenon of active bottlenecks refers to ‘‘maximum flow rates decrease when queues form”. Kinematic wave theories are well-known theories to analyze and simulate the processes of queue formation, propagation, and dissipation via shock and rarefaction waves. Jin [114] studied the merging traffic flow using continuous kinematic wave models.

The kinematic wave model is a first-order quasilinear equation in traffic science and engineering due to its simple mathematical structure and ability to capture realistic traffic networks and shock waves [115]. Under their high efficiency, the kinematic wave is still commonly used in hydrology for flow routing [116]. Conversely, treatment of the kinematic wave model not as a FOQL PDE but a Hamilton-Jacobi type leads to inconsistency as in

Chapter 3 or Mean *et al*. [56]. Those properties are well-known among mathematicians since Oleĭnik [117] established the theory of FOQL PDEs in 1D domains, considering GSs in the space of measurable and bounded functions. Kružkov [118] in 1970 refined the theory in the space of functions of bounded variations (BV functions) in multi-dimensional domains, introducing the notion of the weak entropy solution. Shao *et al*. [119] proved the unique existence of global BV solutions to Cauchy problems for FOQL PDEs with damping if the initial data is non-smooth. Wang [120] demonstrated the unique existence of global BV solutions to Cauchy problems for homogeneous FOQL PDEs if the initial data is BV. In contrast to these intuitively reasonable results, the development of discontinuities under the smoothness of all input is not apparent. Jeffrey [121], Jeffrey [122], and Jeffrey and Donato [123] studied discontinuities in the solutions to Cauchy problems for FOQL PDEs of more than one dependent variable with smooth initial data. Coclite *et al*. [124] considered traffic flows, defined on a road network with junctions, as BV functions. Chen [125] analyzed the formation of shock waves in two-dimensional steady supersonic flows passing around smooth concave walls. This study considers possibly discontinuous measurable and bounded solutions to the kinematic wave model, which governs the wetted cross-sectional area as a scalar dependent variable. We firstly revisit the fundamental mathematical result and then opt for a numerical approach. Numerical examples are computed with the Godunov scheme [126]. The Godunov scheme can capture discontinuities in GSs of FOQL PDEs, such as the traffic flow model of Bretti *et al*. [127]. More details of discretizing FOQL PDEs developing discontinuities from smooth initial data can be found in Fjordholm and Mishra [128].

4.2 Kinematic wave model as a FOQL PDE

The kinematic wave model is a FOQL PDE governing the unknown wetted cross-sectional area $A = A(t,x)$, written as

$$\frac{\partial A}{\partial t} + \frac{\partial Q(x,A)}{\partial x} = q(t,x,A) \tag{4.1}$$

where Q is the discharge given by

$$Q = \frac{1}{n(x)} AR^p \sqrt{S_0(x)} \tag{4.2}$$

where *n* and *p* are the roughness coefficient and the exponent of the friction law, respectively, S_0 (>0) is the channel bed slope, and R is the hydraulic radius depending on x and A. We consider the Cauchy problem of **(4.1)** with **(4.2)** in

$$G = \{(t,x) \mid 0 < t < \infty, -\infty < x < \infty\} \tag{4.3}$$

under the initial condition

$$A(0,x) = A_0(x) \tag{4.4}$$

where $A_0(x)$ is the specified initial value at x. Let $L^1(G)$ and $L^\infty(G)$ be the Lebesgue spaces consisting of all measurable functions and all bounded functions in G, respectively. The space of all infinitely differentiable functions in G is denoted by $C^\infty(G)$. A bounded measurable function $A = A(t,x) \in L^1(G) \cap L^\infty(G)$ such that

$$\iint_G \left(\frac{\partial f}{\partial t} A + \frac{\partial f}{\partial x} Q + fq \right) \mathrm{d}x\mathrm{d}t + \int_{-\infty}^{\infty} f(0,x) A_0(x) \mathrm{d}x = 0 \tag{4.5}$$

for any $f \in C^{\infty}(G)$ having a bounded support is referred to as the GS of the Cauchy problem.

A spatial flow domain is set as $(0, X)$ to prescribe the source term as a distribution

$$\int_{-\infty}^{\infty} f(t,x) q \mathrm{d}x = f(t,0) Q_{\text{in}}(t) - f(t,X) Q_{\text{out}}(t) \tag{4.6}$$

where Q_{in} is the inflow discharge specified at the upstream end $x = 0$, and Q_{out} is the outflow discharge at the downstream end $x = X$ given by

$$Q_{\text{out}}(t) = \lim_{x \to X^-} Q(x, A(t,x)) = \lim_{x \uparrow X} Q(x, A(t,x)) . \tag{4.7}$$

The unknown $A = A(t,x)$ vanishes outside $(0, X)$.

The possibly non-smooth functions q, A_0, etc. are mollified as q^{ρ}, A_0^{ρ}, etc., respectively, by taking convolution with a mollifier φ of radius ρ. A well-known concrete example of a mollifier of radius 1 is

$$\varphi(\xi) = \begin{cases} k \exp\left(-\dfrac{1}{1 - |\xi|^2} \right) & \text{if } |\xi| < 1 \\ 0 & \text{if } |\xi| \geq 1 \end{cases} \tag{4.8}$$

where k is the constant such that $\int_{\mathbb{R}} \varphi(\xi) \mathrm{d}\xi = 1$ [129]. Then, the mollified Cauchy problem fulfills all the regularity assumptions made in Section 2 and Section 4 of Oleĭnik [117], to have a GS $A^{\rho} = A^{\rho}(t,x) \in L^1(G) \cap L^{\infty}(G)$ such that

$$\iint_G \left(\frac{\partial f}{\partial t} A^\rho + \frac{\partial f}{\partial x} Q\left(x, A^\rho\right) + f q^\rho \right) \mathrm{d}x\mathrm{d}t + \int_{-\infty}^{\infty} f(0,x) A_0^\rho(x) \mathrm{d}x = 0 \tag{4.9}$$

for any $f \in C^\infty(G)$ having a bounded support. By the completeness of $L^1(G)$ and $L^\infty(G)$, there exists a unique GS of the original Cauchy problem.

4.3 Godunov scheme

The Godunov scheme is a conservative numerical scheme to approximate the solution of partial differential equations. The conservative scheme leads to a correct propagation speed computation for shock waves or bores. The original Godunov upwind method is first-order accurate in space and time. The Godunov method is one of the more precise methods within the family of first-order schemes, which has the slightest truncation error for linear problems [130]. Two outstanding features of the Godunov method are (i) the use of the conservative form of the equations to produce a relation between integral averages of conserved variables and intercell fluxes and (ii) the use of wave propagation information, upwinding scheme, into the discretization scheme to compute intercell fluxes and thus produce a numerical scheme [105]. Hence, properties derived from the exact local solution of the Euler equations are introduced in the discretization [131]. The Godunov schemes have been successfully applied in engineering (river flows) [132] and traffic flow models [133].

Here, the Godunov scheme is applied to **(4.1)** on the spatial flow domain $(0, X)$, divided into cells of equal length Δx, to update the cell values of the discretized unknown A in a constant time increment Δt, chosen to achieve the stability condition. The scheme defines the numerical flux Q_{f} between adjacent two cells as

$$Q_{\mathrm{f}} = \begin{cases} Q_L & \text{if } A_L \geq A_R \text{ and } Q_L \geq Q_R \\ Q_R & \text{if } A_L \geq A_R \text{ and } Q_L \leq Q_R \\ Q_L & \text{if } A_L \leq A_R \text{ and } \left(\partial Q/\partial A\right)_L \geq 0 \\ Q_R & \text{if } A_L \leq A_R \text{ and } \left(\partial Q/\partial A\right)_R \leq 0 \\ 0 & \text{otherwise} \end{cases} \tag{4.10}$$

where the subscripts L and R represent the values in the left-side cell and the right-side cell, respectively. The last case of **(4.10)** stems from $Q\left(x, Q^{-1}(0)\right) = 0$. Then, the cell value $A^{(n)}$ at n-th time step is updated as

$$A^{(n+1)} = A^{(n)} - \frac{\Delta t}{\Delta x}\Delta Q_{\mathrm{f}} \tag{4.11}$$

where ΔQ_{f} is the difference between the two fluxes Q_{f} associated with the cell.

4.4 Numerical demonstrations and discussion

Two numerical examples, referred to as Case 1 and Case 2, are presented. Case 1 deals with the practical problem of abrupt water release from Chan Thnal Reservoir into an initially dry bed of the 7320 (m) long irrigation canal discussed in Chapter 3 [56]. Case 2 deals with a hypothetical problem under the smoothness of all input. In both cases, the friction law is

prescribed as $n = 0.03$ ($m^{-1/3}s$) and $p = 2/3$, and the initial condition is specified as the very shallow water of $A_0 = 10^{-6}$ (m^2) in $(0, X)$.

4.4.1 Case 1

The spatial flow domain $(0, X)$ is set as $(0, 7320)$, and the bed slopes are piecewise constant in the five reaches as defined in Chapter 3. However, the irrigation canal's cross-sectional shape, which was considered very broad rectangular in Chapter 3, is now assumed to be trapezoidal with a side slope of 1:1 and a bottom width $B_1 = 10$ (m). Therefore, the water depth h and the cross-sectional area A are converted to each other with smooth relationships $A = B_1 h + 0.5h^2$ and $h = \sqrt{B_1^2 + 2A} - B_1$. The mesh sizes are set as $\Delta x = 10$ (m) and $\Delta t = 0.1$ (s). The inflow discharge at the upstream end $x = 0$ is $Q_{in} = 80$ (m^3/s) for $0 < t < 3600$ (s) and then abruptly turns into $Q_{in} = 0$ for $3600 \le t$. **Figure 4.1** shows the hydrographs of discharges Q_{in}, computed Q_f at the four changing points of the bed slopes, and Q_{out} for $0 \le t \le 21600$ (s). The wavefront remains abrupt, while the tail decays as propagating downstream. **Figure 4.2** depicts the temporally evolving profiles of the cross-sectional areas over the spatial flow domain of the varied bed slopes. The hydrographs of the cross-sectional areas at the changing points of bed slopes are shown in **Figure 4.3**. The cross-sectional areas in **Figure 4.2** and **Figure 4.3** are converted to water depths in **Figure 4.4** and **Figure 4.5**, respectively. Unlike the level-set method in Chapter 3, the approach with the

FOQL PDE in this chapter successfully reproduces the surface water flows over the varied bed slopes with correct mass conservation.

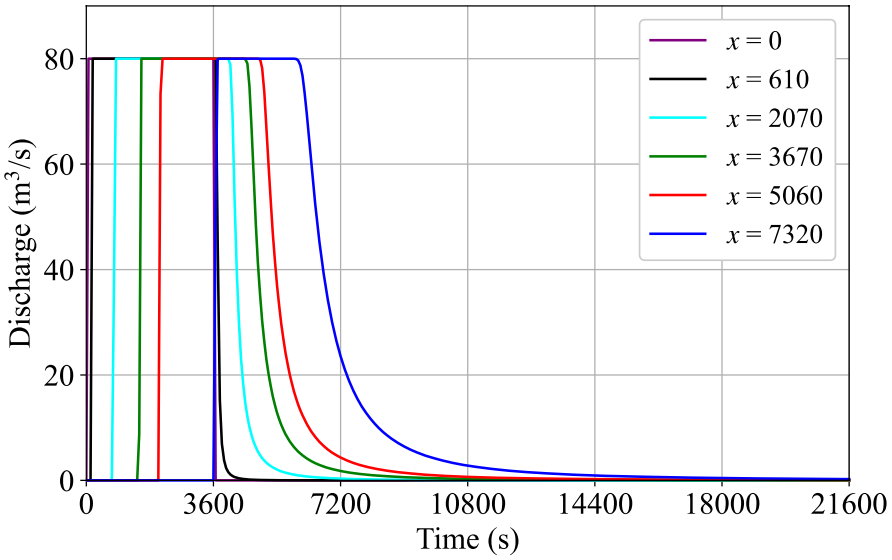

Figure 4.1. Hydrographs of discharges at different locations in the spatial flow domain for Case 1 with abrupt changes in the bed slope and the inflow discharge.

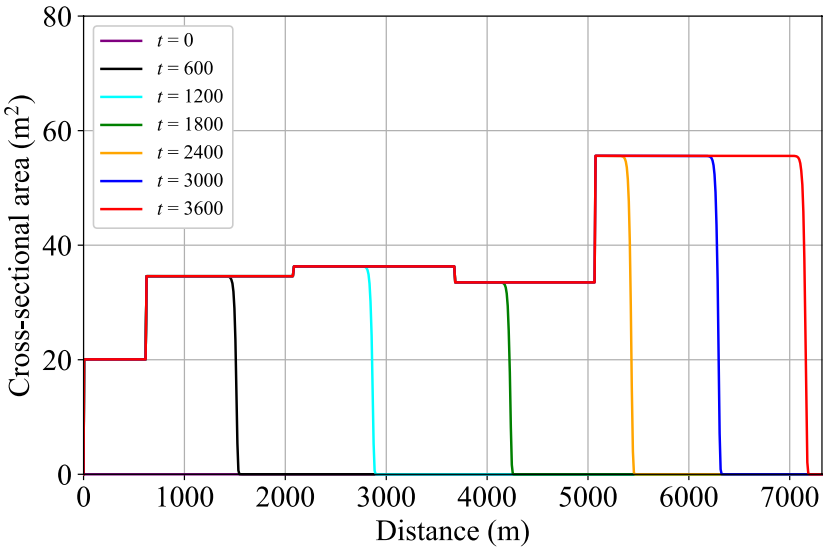

Figure 4.2. Variations of cross-sectional areas at different times in the spatial flow domain for Case 1 with abrupt changes in the bed slope.

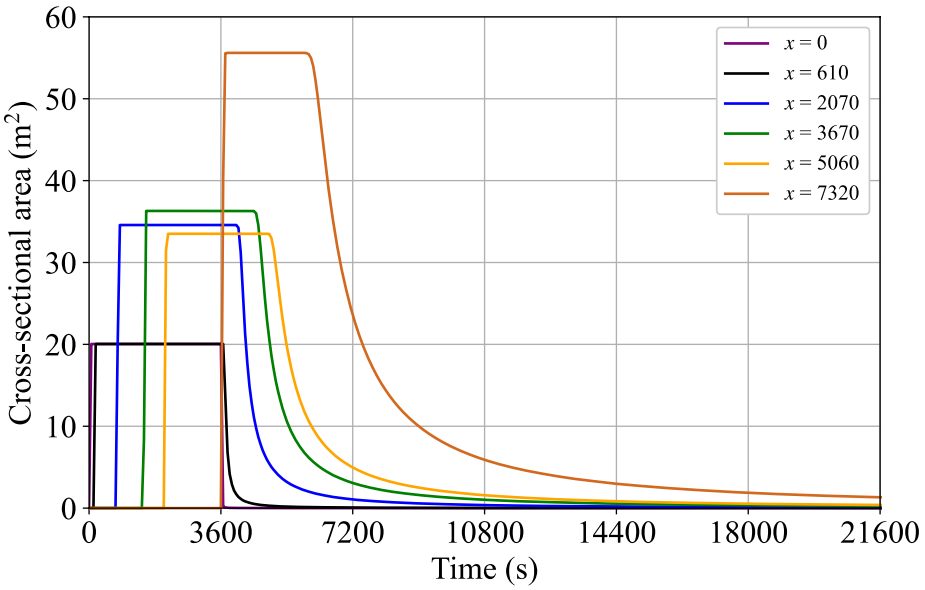

Figure 4.3. Hydrographs of cross-sectional areas at different locations in the spatial flow domain for Case 1 with abrupt changes in the bed slope.

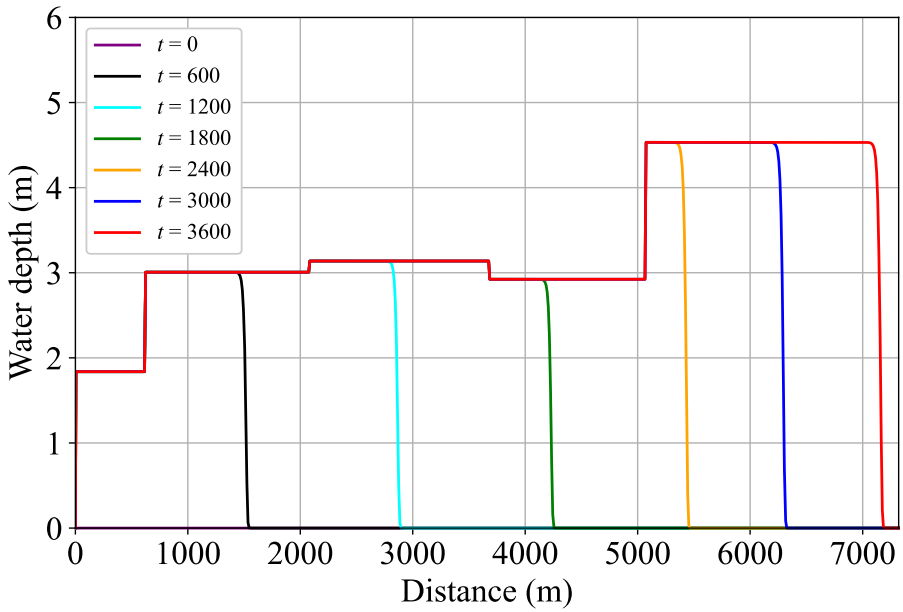

Figure 4.4. Variations of water depths at different times in the spatial flow domain for Case 1 with abrupt changes in the bed slope.

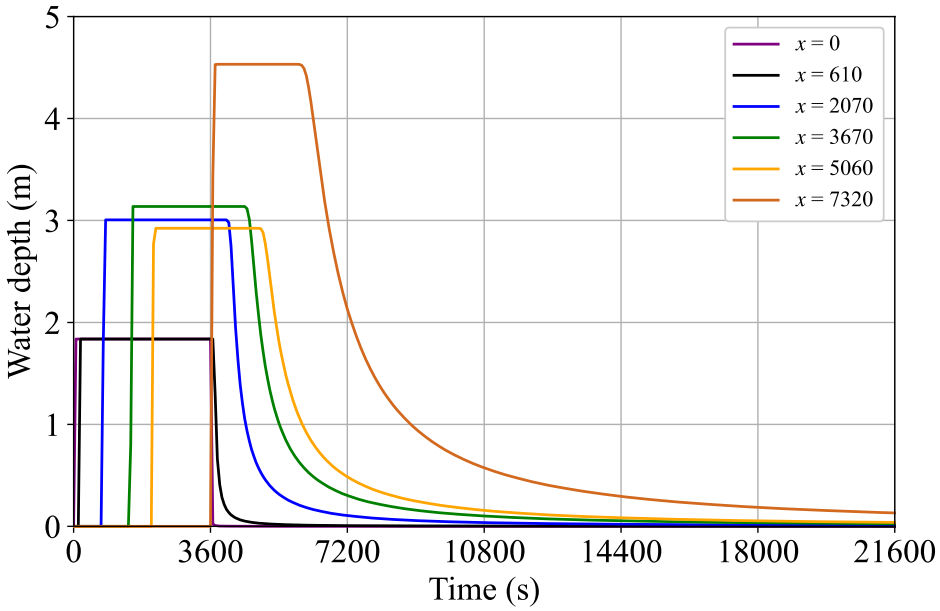

Figure 4.5. Hydrographs of water depths at different locations in the spatial flow domain for Case 1 with abrupt changes in the bed slope.

4.4.2 Case 2

The hypothetical problem of Case 2 assumes $X = 2000$ (m), with the mesh sizes $\Delta x = 2$ (m) and $\Delta t = 0.4$ (s). The bed slopes are prescribed as $S_0(x) = 10^{-3-\cos(\pi x/1000)}$ so that the bed elevation becomes a smooth concave function of x. The smooth inflow discharge at the upstream end $x = 0$ is specified as $Q_{\text{in}} = 0.04\left[\varphi\left((t-600)/600\right)\right]/k$ (m^3/s) using the example of a mollifier where $k = 2.2523$. **Figure 4.6** shows the hydrographs of discharges at Q_{in}, computed Q_{f} at $x = 500$ (m), $x = 1000$ (m), $x = 1500$ (m), and Q_{out} for $0 \le t \le 6000$ (s). The shock wave develops and it is clearly visible from one position to another. Furthermore, with a possible analogy to the study of Chen [125], **Figure 4.6** exhibits

oscillations, including abrupt decreases in the discharges appearing in the tails as the shock wave propagates downstream, passing through the point of the steepest bed slope.

The maximum increments of discharges within 25j time steps, denoted by ΔQ_{Mj}, are depicted in **Figure 4.7** for j = 1, 3, and 5. For all j time steps, ΔQ_{Mj} increases with the position. It indicates that the maximum increments between the discharge at a next time step is getting larger than the current time step when ΔQ_{Mj} is moving downstream. Consequently, **Figure 4.6** and **Figure 4.7** indicate the formation of a shock wave having an abrupt wavefront without any dissipation.

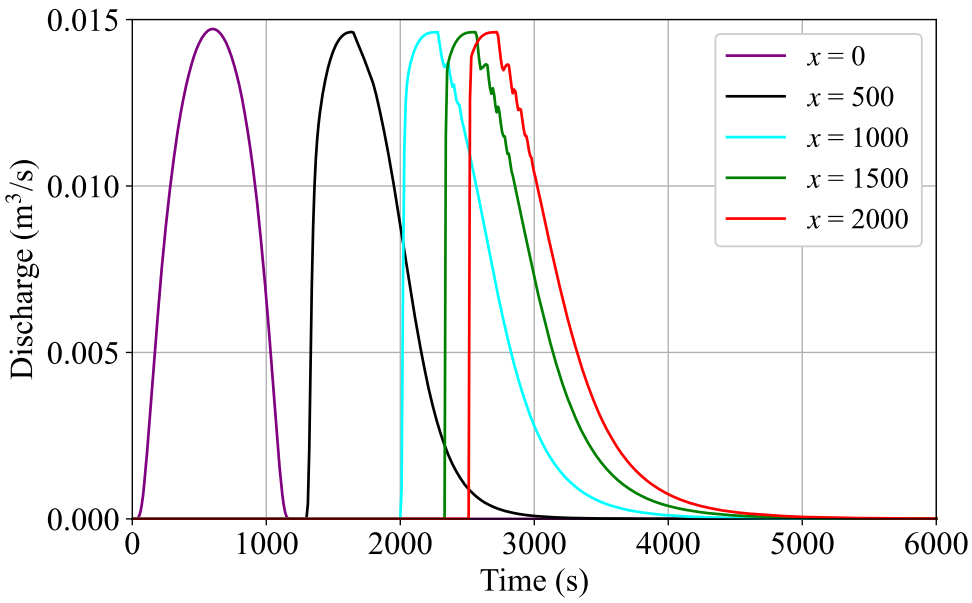

Figure 4.6. Hydrographs of discharges at different locations in the spatial flow domain for Case 2 under the smoothness of all input data.

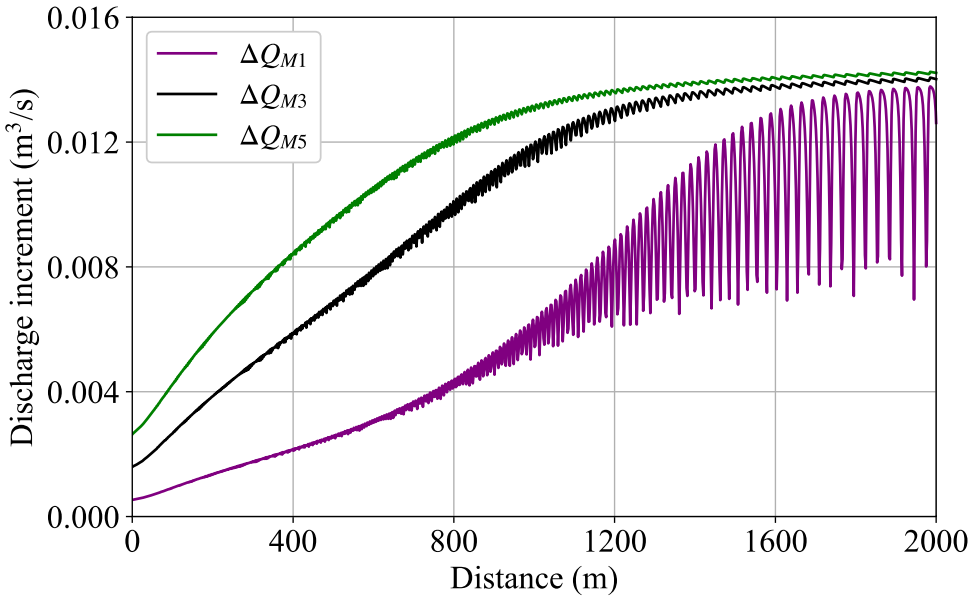

Figure 4.7. Maximum increments ΔQ_{Mj} of discharges within 25j time steps for j = 1, 3, and 5 at each point of the spatial flow domain in Case 2.

4.5 Conclusions

The fundamental properties of FOQL PDEs implicate the existence of non-dissipating discontinuous kinematic waves. The numerical examples presented in this chapter support the hypothesis that such discontinuities in kinematic waves develop from the discontinuities of input data or even under the smoothness of all input. The numerical demonstration of Chan Thnal irrigation canal (Case 1) representing the discontinuities of all input is successfully computed the solutions of the surface water flows when the bed slopes vary. The hypothetical problem (Case 2) delineates that the non-dissipative discontinuous kinematic waves emerge under the smoothness of all input. Abrupt arrivals of flash floods are reported mostly in arid regions where concave topographies are typical [134], making a real-world manifestation of

the phenomena presented here. However, rigorous mathematical analysis is still necessary to prove that the numerically obtained abrupt changes are valid evidence of the discontinuities.

Chapter 5

5 A thorough description of one-dimensional steady open channel flows using the notion of discontinuous viscosity solution

5.1 Introduction

Open channel flows in dominantly 1D channels are of practical importance in civil engineering applications. The governing equations of 1D open channel flows are derived from the SWEs, constituting a hyperbolic system of first-order PDEs to represent the conservation laws of mass and momentum in fluid mechanics. The SWEs imply that a discontinuity of water depths, referred to as a hydraulic jump or shock, may occur under the Rankine–Hugoniot condition.

Tremendous efforts have been devoted to initial-boundary value problems of the SWEs in bounded domains, primarily for the numerical solution of unsteady states. Toro and Garcia-Navarro [105] thoroughly reviewed Godunov-type methods applied to SWEs, mentioning the critical points such as the jump conditions and the presence of source terms. As far as numerical methods for 1D problems are concerned, careful considerations on moving fronts [135] and on balancing source terms and flux gradients [67] have resulted in significant advances [63]. However, there remain mathematical fundamentals involving the 1D SWEs, and several recent papers highlighted the approximation of the 1D SWEs. Cheutouf and Smaoui [136] discussed the well-posedness in diffusion wave approximation of the 1D SWEs. Mean et al. [56], which has been described in Chapter 3, explored the applicability of the level-set methods to kinematic wave approximation of the 1D SWEs. Sukhtayev et al. [137] investigated water surface profiles, which may be non-smooth or discontinuous, in the framework of a generalized Sturm-Liouville problem reduced from the stability problem of the 1D SWEs.

More emphasis should be placed on analyzing 1D open channel flows in steady states, as the hydraulic design of rivers, irrigation canals, and sewer systems often based on them with the possible inclusion of control devices such as gates and weirs to regulate the water flows. Simply dropping the unsteady terms of the 1D SWEs results in the SFO ODE on which we should focus in this chapter. A significant difficulty is determining 1D steady open channel flows in a domain bounded by two water level control devices involving a Dirichlet problem of the SFO ODE constraining water depths at the two boundary points. Such a two-point boundary value problem is mathematically ill-posed unless admitting a discontinuity in the water depths.

Adding a virtual unsteady term to the SFO ODE might be a viable approach, as it constitutes a FOQL PDE representing a scalar conservation law. There are several mathematical notions to deal with non-smooth or discontinuous solutions of FOQL PDEs. Oleĭnik [117] established GSs of FOQL PDEs as the limit functions of the solutions to parabolic PDEs, namely, using the method of vanishing viscosity. Kružkov [118] refined that notion of GS in the space of functions of bounded variation (BV). Jerez and Arciga [138] called such a GS as the BV entropy weak solution, which is required to achieve the uniqueness of a physically reasonable solution to a FOQL PDE representing a scalar conservation law. Glaubitz [139] developed a shock-capturing procedure for the stable numerical approximation of BV entropy weak solutions to FOQL PDEs. Functions of BV are also appropriate for different applications, such as value functions of optimal control problems [100] and total variation flows [140]. However, it is challenging to clarify whether such a BV entropy solution exists globally in time and converges to a steady-state as time goes by or not.

An option comprehending SFO ODEs and FOQL PDEs is to regard them as equations of Hamilton-Jacobi type (HJ equations). In the 1980s, Crandall and Lions [37] introduced the notion of VS for HJ equations, considering both steady Dirichlet problems and unsteady Cauchy problems. A VS is obtained not only via the method of vanishing viscosity but also the finite difference method [141], via Perron's method [52], and as the value function of the associated optimal control problem [142]. Barles [54] proved existence for those two problems of HJ equations, whose VSs are possibly discontinuous. Barles and Perthame [45] focused on possibly discontinuous VSs of the Dirichlet problems associated with deterministic optimal stopping time problems, which can be approached via the method of

vanishing viscosity [143]. However, as revisited in the 1990s [44,144], well-posed Dirichlet problems of HJ equations require certain structural assumptions on the Hamiltonian functions, such as proper dependence on the unknown variable. In such well-structured cases, the link between VSs of HJ equations and BV entropy solutions of FOQL PDEs representing scalar conservation laws has been known [145]. On the other hand, the HJ equation accommodated to the SFO ODE for the 1D steady open channel flows has an essentially improper Hamiltonian function, where relaxation as in Unami and Mohawesh [146] is not applicable. Therefore, we cannot expect a comparison principle to guarantee the uniqueness and stability of a VS. However, we have the advantage of already knowing several types of 1D steady open channel flows, which can be seen in the standard textbooks of open channel hydraulics [32,147].

In this chapter, we use the notion of VS to describe the characteristics of the 1D steady open channel flows as the solutions to Dirichlet problems of SFO ODEs, even though the method of vanishing viscosity does not work due to the structure of the Hamiltonian function hindering the solution of a relevant two-point boundary value problem of a second-order ODE [148]. It is shown that the discontinuous VSs to the Dirichlet problems satisfy the entropy condition, with which the BV entropy weak solutions accompany, and are GSs in the Oleĭnik [117]'s sense. VSs to some Dirichlet problems are indeed not unique, and a concrete illustrative example is presented.

5.2 Preliminaries

We consider open channel flows subject to the following physical assumptions **A1**-**A5**.

A1. The channel is prismatic, having a straight alignment and a constant cross-sectional shape.

A2. The channel bed slope $S_0 = \tan\theta$ is so small that the approximations $\theta = \sin\theta = \tan\theta$ and $\cos\theta = 1$ are acceptable.

A3. The pressure distribution is hydrostatic.

A4. The velocity distribution in a channel cross-section is uniform.

A5. The friction force is the same as in uniform flows, and it is represented as the friction slope.

5.2.1 Conventional governing equations of 1D open channel flows

The conservation laws of mass and momentum under the assumption of **A1**-**A5** are summarized as the 1D SWEs without the lateral inflow discharge per unit width q

$$\frac{\partial}{\partial t}\begin{pmatrix} A \\ Q \end{pmatrix} + \frac{\partial}{\partial x}\begin{pmatrix} Q \\ F_s \end{pmatrix} = \begin{pmatrix} 0 \\ gA\left(S_0 - S_f\right) \end{pmatrix} \tag{5.1}$$

where F_s is the specific force given by

$$F_s = \frac{Q^2}{A} + \int_0^h g\frac{\partial A}{\partial z}\left(h - z\right)\mathrm{d}z \tag{5.2}$$

and the friction slope is

$$S_f = S_f(h) = \frac{n^2 Q|Q|}{A^2 R^{2p}} \tag{5.3}$$

where h is the water depth, $A = A(h)$ is the wetted cross-sectional area, Q is the discharge, $R = A/P$ is the hydraulic radius with the wetted perimeter $P = P(h)$, n is the roughness coefficient, z is the upward vertical axis, and p is the exponent as in the uniform flow formula.

The 1D SWEs **(5.1)** in steady states indicate that the discharge Q is constant and that

$$\frac{\mathrm{d}F_s}{\mathrm{d}x} = \frac{\mathrm{d}}{\mathrm{d}x}\left(\frac{Q^2}{A} + \int_0^h g \frac{\partial A}{\partial z}(h - z)\,\mathrm{d}z \right) = gA\left(S_0 - S_f\right) \tag{5.4}$$

which is formally rewritten as a non-conservative form

$$\left(gA - \frac{\partial A}{\partial h}\frac{Q^2}{A^2} \right)\frac{\mathrm{d}h}{\mathrm{d}x} = gA\left(S_0 - S_f\right). \tag{5.5}$$

A water depth h_{uni} achieving $S_f\left(h_{\mathrm{uni}}\right) = S_0$ is referred to as the uniform flow depth. The commonly used governing equation of 1D steady open channel flows obtained from **(5.5)** as

$$\frac{\mathrm{d}h}{\mathrm{d}x} = \frac{S_0 - S_f}{1 - Fr^2} \tag{5.6}$$

where Fr is the Froude number defined by

$$Fr = \sqrt{\frac{\partial A}{\partial h}\frac{Q^2}{gA^3}}. \tag{5.7}$$

A water depth h_{cri} achieving $Fr\left(h_{\mathrm{cri}}\right) = 1$ is referred to as the critical flow depth. It is known that the water depths h gradually varying along the channel satisfy the SFO ODE **(5.6)**, which does not explain the occurrence of a hydraulic jump.

The Froude number can distinguish the flow types as

- Subcritical flow when $Fr < 1$
- Critical flow when $Fr = 1$
- Supercritical flow when $Fr > 1$.

The equation **(5.6)** describes the variation of the flow depth with respect to space coordinate, known as the longitude of the channel. It is used to characterize the water surface profiles of the open channel flows. However, it does not explain the occurrence of a hydraulic jump.

In the open channel flows, a channel transition may involve changing the channel geometry, which is the change of the channel width or the channel bottom slope [31]. The bottom slope is classified by critical water depth (h_{cri}) and normal water depth (h_{uni}) into five categories: mild, steep, critical, horizontal, and adverse. The bottom slope is called mild if the uniform flow is subcritical ($h_{\text{uni}} > h_{\text{cri}}$), steep if the uniform flow is supercritical ($h_{\text{uni}} < h_{\text{cri}}$), critical if the uniform flow is critical ($h_{\text{uni}} = h_{\text{cri}}$), horizontal if the slope is zero, and adverse if the slope is negative. Various kinds of bottom slopes produce different water surface profiles. Another critical factor to characterize the water surface profiles is where the water surface is located, referring to regions. The regions of the water surface profiles are notified based on the location of the critical-depth line (CDL) and uniform-depth line (UDL), which are critical water depth (h_{cri}) and normal water depth (h_{uni}), respectively. The region above both lines is referred to as Zone 1 $(h > h_{\text{uni}} > h_{\text{cri}})$ or $(h > h_{\text{cri}} > h_{\text{uni}})$; between both

lines is Zone 2 $(h_{uni} > h > h_{cri})$ or $(h_{cri} > h > h_{uni})$; the one between the lower line and the channel bottom is designated as Zone 3 $(h_{uni} > h_{cri} > h)$ or $(h_{cri} > h_{uni} > h)$, as shown in **Figure 5.1**.

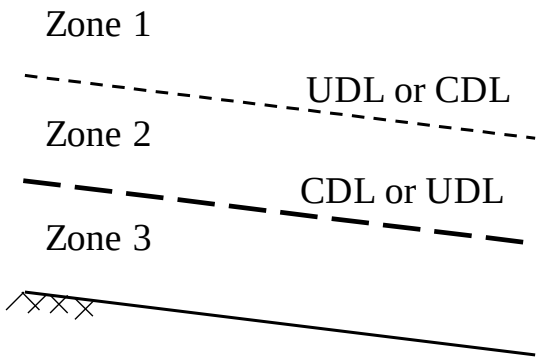

Figure 5.1. Zones of the water surface profiles.

5.2.2 Spaces of functions

Henceforth, we utilize several spaces of functions of a generic independent variable a. Functions are collectively denoted by $v = v(a)$. Let Ω be an open a-domain in $\mathbb{R}$. The space $C_B(\Omega)$ consisting of all bounded and continuous functions on Ω is complete with respect to the uniform norm $\|v\|_\infty = \sup_{a\in\Omega} |v(a)|$. The space $C(\overline{\Omega})$ consisting of all bounded and uniformly continuous functions on Ω is a closed subspace of $C_B(\Omega)$. The space $C^1(\Omega)$ consists of all continuous functions whose first derivatives are also continuous on Ω. The space $C_B^1(\Omega)$ consists of all bounded and continuous functions whose first derivatives are also bounded and continuous on Ω and is complete with respect to the norm

$\|v\|_{C_B^1} = \max\left(\|v\|_\infty, \|\mathrm{d}v/\mathrm{d}a\|_\infty\right)$. The spaces of upper and lower semi-continuous functions defined on $\overline{\Omega}$ are denoted by $USC\left(\overline{\Omega}\right)$ and $LSC\left(\overline{\Omega}\right)$, respectively. The space $L^1(\Omega)$ is the Lebesgue space of all integrable functions v on Ω, equipped with the norm

$$\|v\|_{L^1} = \int_\Omega |v| \, \mathrm{d}\Omega. \tag{5.8}$$

The space $W^{1,1}(\Omega)$ is the Sobolev space, which is the completion of $C^1\left(\Omega\right)$ with respect to the norm

$$\|v\|_{1,1} = \|v\|_{L^1} + \left\|\frac{\mathrm{d}v}{\mathrm{d}a}\right\|_{L^1}. \tag{5.9}$$

The space $W^{1,\infty}(\mathbb{R})$ is the Sobolev space, which is the completion of $C^1\left(\mathbb{R}\right)$ with respect to the norm

$$\|v\|_{1,\infty} = \max\left(\operatorname*{ess\,sup}_{a\in\mathbb{R}} |v(a)|, \operatorname*{ess\,sup}_{a\in\mathbb{R}} \left|\frac{\mathrm{d}v}{\mathrm{d}a}(a)\right|\right). \tag{5.10}$$

5.2.3 The notion of discontinuous VS

In this study, we regard **(5.5)** as an HJ equation

$$H\left(u, \frac{\mathrm{d}u}{\mathrm{d}x}\right) = 0 \tag{5.11}$$

where H is the Hamiltonian function, in a bounded open x-domain Ω. The definition of VS here is adapted the discontinuous viscosity from [41]. The upper semi-continuous envelope (U-env) $u^*(x)$ of a function $u(x)$ is defined as

$$u^*(x) = \limsup_{y \to x} u(y). \tag{5.12}$$

The lower semi-continuous envelope (L-env) $u_*(x)$ of a function $u(x)$ is defined as

$$u_*(x) = \liminf_{y \to x} u(y). \tag{5.13}$$

There is a trivial comparison principle

$$u_*(x) \le u(x) \le u^*(x) \tag{5.14}$$

at any $x \in \Omega$. The U-env $u^*(x) \in USC(\overline{\Omega})$ is called a viscosity sub-solution (sub-S) of **(5.11)** if, for any weight $w \in C^1(\Omega)$,

$$H\left(u^*(x), \frac{\mathrm{d}w(x)}{\mathrm{d}x}\right) \le 0 \tag{5.15}$$

holds at any point x where $u^* - w$ achieves a local maximum. The L-env $u_*(x) \in LSC(\overline{\Omega})$ is called a viscosity super-solution (super-S) of **(5.11)** if, for any weight $w \in C^1(\Omega)$,

$$H\left(u_*(x), \frac{\mathrm{d}w(x)}{\mathrm{d}x}\right) \ge 0 \tag{5.16}$$

holds at any point x where $u_* - w$ achieves a local minimum. When the U-env u^* and the L-env u_* of a function $u(x)$ are a sub-S and a super-S, respectively, $u(x)$ is called a VS of **(5.11)** in Ω.

5.3 Problem formulation and mathematical analysis

5.3.1 Statement of problems

Firstly, we transform the unknown variable, the water depth h, as

$$u = \log h \tag{5.17}$$

so that the range of the unknown u becomes $\mathbb{R}$. The uniform flow depth and the critical flow depth are transformed as $u_{\text{uni}} = \log h_{\text{uni}}$ and $u_{\text{cri}} = \log h_{\text{cri}}$, respectively. The flux $\varphi(u)$ is the negative specific force

$$\varphi(u) = -F_s = -\frac{Q^2}{A} - \int_0^h g\frac{\partial A}{\partial z}(h-z)\,\mathrm{d}z \tag{5.18}$$

and it is assumed that $\varphi(u) \in W^{1,\infty}(\mathbb{R})$, φ_u is strictly monotone decreasing, and thus

$$\varphi_{uu}(u) < 0 \tag{5.19}$$

almost everywhere. The source term $\psi(u)$ is the external force

$$\psi(u) = gA\left(S_0 - S_f\right) \tag{5.20}$$

which is assumed to be in $W^{1,\infty}(\mathbb{R})$.

We pose the following three problems considering different senses of solutions.

Problem 1. Find a gradually varied flow solution (GVFS) $u(x) \in C_B^1(\Omega)$ of

$$H\left(u, \frac{\mathrm{d}u}{\mathrm{d}x}\right) = \varphi_u(u)\frac{\mathrm{d}u}{\mathrm{d}x} + \psi(u) = \left(Fr^2(u) - 1\right)e^u\frac{\mathrm{d}u}{\mathrm{d}x} + S_0 - S_f(u) = 0 \tag{5.21}$$

in $\Omega=(0,X)=(0,|X|)$ or $\Omega=(X,0)=(-|X|,0)$ with a free endpoint X, satisfying the Dirichlet boundary condition

$$u(0)=u_{\mathrm{up}},\quad u(X)=u_{\mathrm{down}} \tag{5.22}$$

where u_{up} and u_{down} are specified boundary values.

Problem 2. Find a VS $u(x)\in L^1(\Omega)\cap L^\infty(\Omega)$ of **(5.21)** in $\Omega=(0,X)$ with a specified downstream endpoint X, satisfying the Dirichlet boundary condition

$$u^*(0)=u(0)=u_*(0)=u_{\mathrm{up}},\quad u^*(X)=u(X)=u_*(X)=u_{\mathrm{down}} \tag{5.23}$$

where u_{up} and u_{down} are specified boundary values.

Problem 3. Find a GS $u(x)\in L^1(\Omega)\cap L^\infty(\Omega)$, where $\Omega=(0,X)$, such that

$$\int_0^X\left(\varphi(u)\frac{\mathrm{d}f}{\mathrm{d}x}-\psi(u)f\right)\mathrm{d}x+f(0)\varphi(u_{\mathrm{up}})-f(X)\varphi(u_{\mathrm{down}})=0 \tag{5.24}$$

for any $f\in W^{1,1}(\Omega)$.

5.3.2 Unique existence of GVFSs

Firstly, we clarify the unique existence of the conventional GVFSs as solutions to **Problem 1**.

Theorem 1. Let $\Omega=(u_{\mathrm{up}},u_{\mathrm{down}})$. If the closed interval $\overline{\Omega}$ does not contain any u_{uni} and if $\varphi_u(u)$ is continuous in Ω, then there exists unique $x(u)\in C(\overline{\Omega})$ such that

$$x(u) = \int_{u_{\text{up}}}^{u} -\frac{\varphi_u(u)}{\psi(u)}\,\mathrm{d}u = \int_{u_{\text{up}}}^{u} \frac{1-Fr^2}{S_0 - S_f}\frac{\mathrm{d}h}{\mathrm{d}u}\,\mathrm{d}u\,. \tag{5.25}$$

Proof. As $\psi(u) \neq 0$, **(5.21)** can be rewritten as $\mathrm{d}x/\mathrm{d}u = e^u\left(1-Fr^2\right)/\left(S_0 - S_f\right)$ and then

$$\frac{\mathrm{d}x}{\mathrm{d}h} = \frac{1-Fr^2}{S_0 - S_f} \tag{5.26}$$

whose right-hand side is Lipschitz continuous with respect to x with any Lipschitz constant. Then, the unique existence of $x(u) \in C(\overline{\Omega})$ such that **(5.25)** is a direct consequence of the well-known result for initial value problems of ODEs (Theorem 1.1.1 of [148]).

□

Remark 1. In $\Omega = (0, X) = (0, |X|)$ or $\Omega = (X, 0) = (-|X|, 0)$, there exist unique monotone GVFS $u(x) \in C_B^1(\Omega)$ solving **Problem 1** with $X = x(u_{\text{down}})$ determined by **(5.25)**, if the closed interval $\left[u_{\text{up}}, u_{\text{down}}\right]$ does not contain any u_{uni} or u_{cri} and if $\varphi_u(u)$ is continuous in $\left(u_{\text{up}}, u_{\text{down}}\right)$. There is a comparison principle that the solution $u(x)$ is bounded as

$$\min\left(u_{\text{up}}, u_{\text{down}}\right) \leq u(x) \leq \max\left(u_{\text{up}}, u_{\text{down}}\right). \tag{5.27}$$

Remark 2. The uniform flow $u(x) = u_{\text{uni}} \in C_B^1(\Omega)$ solves **Problem 1** with the boundary value specified as $u_{\text{up}} = u_{\text{down}} = u_{\text{uni}}$.

5.3.3 Properties of VSs

Next, properties of VSs, which are possibly non-smooth or discontinuous, are explored. It is observed that there are continuous VSs.

Remark 3. A GVFS $u(x) \in C_B^1(\Omega)$ solving **Problem 1** is a VS solving **Problem 2**.

Remark 4. Suppose $u_{\text{cri}} = u_{\text{uni}}$, that $\lim_{u \to u_{\text{cri}}^{\pm}} \varphi_{uu}(u)$ exists and is finite for either sign, and $\lim_{u \to u_{\text{uni}}^{\pm}} \psi_u(u) \neq 0$ for the sign. Then,

$$\lim_{u_{\text{down}} \to u_{\text{uni}}^{\pm}} \frac{1 - Fr^2}{S_0 - S_f} \frac{\mathrm{d}h}{\mathrm{d}u} = -\frac{\lim_{u_{\text{down}} \to u_{\text{cri}}^{\pm}} \varphi_{uu}(u_{\text{down}})}{\lim_{u_{\text{down}} \to u_{\text{uni}}^{\pm}} \psi_u(u_{\text{down}})} \tag{5.28}$$

for the sign becomes finite, allowing $x(u_{\text{cri}})$ in **(5.25)** to converge to a finite $\xi \subset \mathbb{R}$. Let $u_{\text{GV}}(x)$ denote such a GVFS approaching to $u_{\text{cri}} = u_{\text{uni}}$ at ξ. With another boundary $X \subset \mathbb{R}$ such that $0 < \xi X$ and $|\xi| < |X|$,

$$u(x) = \begin{cases} \begin{cases} u_{\text{GV}}(x) & \text{in } [0, \xi) \\ u_{\text{uni}} & \text{in } [\xi, X] \end{cases} & \text{if } 0 < \xi \\ \begin{cases} u_{\text{uni}} & \text{in } [X, \xi] \\ u_{\text{GV}}(x) & \text{in } (\xi, 0] \end{cases} & \text{if } \xi < 0 \end{cases} \tag{5.29}$$

becomes a VS in $C_B(\Omega)$.

Discontinuities in VSs, which are indeed GSs, are characterized in the following theorems.

Theorem 2. Let $u(x)$ be a VS solving **Problem 2**. Suppose $u^*(\xi) \neq u_*(\xi)$ at a point $\xi \subset \Omega$ and that $\varphi_u(u)$ is continuous at $u^*(\xi)$ and $u_*(\xi)$. For the sub-S $u^*(x) \in USC\left(\overline{\Omega}\right)$ and the super-S $u_*(x) \in LSC\left(\overline{\Omega}\right)$,

$$\varphi_u(u^*(\xi)) < 0, \quad \varphi_u(u_*(\xi)) > 0 \tag{5.30}$$

and $u(x) \in C_B(0,\xi) \cap C_B(\xi, X)$, implying $\varphi_u(u_{\text{up}}) \geq 0$ and $\varphi_u(u_{\text{down}}) \leq 0$.

Proof. Let w be any weight in $C^1(\Omega)$. If $\varphi_u(u^*) \geq 0$ and $u^* - w$ achieves a local maximum at ξ, then $u^*(\xi) < u_*(\xi)$. This contradicts the comparison principle **(5.14)**. If $\varphi_u(u_*) \leq 0$ and $u_* - w$ achieves a local minimum at ξ, then $u^*(\xi) < u_*(\xi)$. This contradicts the comparison principle **(5.14)**. Therefore, **(5.30)** holds. The assumption **(5.19)** implies that φ_u is monotone decreasing, and thus there can be at most one point ξ achieving **(5.30)**. With **Remark 1** and **Remark 4**, it is concluded that $u(x) \in C_B(0,\xi) \cap C_B(\xi, X)$, $\varphi_u(u_{\text{up}}) \geq 0$ and $\varphi_u(u_{\text{down}}) \leq 0$.

□

Theorem 3. Let $u(x)$ be a VS solving **Problem 2**. Suppose that $\varphi_u(u)$ is continuous except at the points of non-smoothness mentioned in **Remark 4** and **Theorem 2**, if any. Then, $u(x)$ is a GS satisfying **(5.24)** for any weight $f \in W^{1,1}(\Omega)$, and

$$\varphi(u^*(\xi)) = \varphi(u_*(\xi)) \tag{5.31}$$

if there is any discontinuity at $\xi \in \Omega$ such that $u^*(\xi) \neq u_*(\xi)$.

Proof. Because of $u(x) \in C_B(0,\xi) \cap C_B(\xi, X)$,

$$
\begin{aligned}
0 &= \int_0^{\xi} f\left(\varphi_u \frac{\mathrm{d}u}{\mathrm{d}x} + \psi\right)\mathrm{d}x + \int_{\xi}^{X} f\left(\varphi_u \frac{\mathrm{d}u}{\mathrm{d}x} + \psi\right)\mathrm{d}x \\
&= \int_0^{\xi}\left(f\varphi_u \frac{\mathrm{d}u_*}{\mathrm{d}x} + f\psi\right)\mathrm{d}x + \int_{\xi}^{X}\left(f\varphi_u \frac{\mathrm{d}u^*}{\mathrm{d}x} + f\psi\right)\mathrm{d}x \\
&= \int_0^{\xi}\left(f\frac{\mathrm{d}\varphi(u_*)}{\mathrm{d}x} + f\psi(u_*)\right)\mathrm{d}x + \int_{\xi}^{X}\left(f\frac{\mathrm{d}\varphi(u^*)}{\mathrm{d}x} + f\psi(u^*)\right)\mathrm{d}x \\
&= f(\xi)\varphi(u_*(\xi)) - f(0)\varphi(u_*(0)) - \int_0^{\xi}\left(\varphi(u_*)\frac{\mathrm{d}f}{\mathrm{d}x} - \psi(u_*)f\right)\mathrm{d}x \\
&\quad - f(\xi)\varphi(u^*(\xi)) + f(X)\varphi(u^*(X)) - \int_{\xi}^{X}\left(\varphi(u^*)\frac{\mathrm{d}f}{\mathrm{d}x} - \psi(u^*)f\right)\mathrm{d}x \\
&= f(X)\varphi(u_{\mathrm{down}}) - f(0)\varphi(u_{\mathrm{up}}) - \int_0^{X}\left(\varphi(u)\frac{\mathrm{d}f}{\mathrm{d}x} - \psi(u)f\right)\mathrm{d}x \\
&\quad + f(\xi)\left(\varphi(u_*(\xi)) - \varphi(u^*(\xi))\right)
\end{aligned}
\tag{5.32}
$$

for any weight $f \in W^{1,1}(\Omega)$. Taking a particular weight $f \in W^{1,1}(\Omega)$ as

$$
f = \lim_{\varepsilon \to 0^+} \max\left(0, 1 - \frac{|\xi - x|}{\varepsilon}\right) \tag{5.33}
$$

results in **(5.31)**. Then, **(5.32)** turns out **(5.24)**.

□

5.3.4 Non-uniqueness of GSs

Lastly, we show that there is a case where GSs are not unique, using auxiliary functions stemming from two different functions $u_1(x)$ and $u_2(x)$ with their mollification. A mollifier $J_\rho(x)$ is defined on $\mathbb{R}$ as

$$J_\rho(x) = 0 \text{ if } |x| \geq \rho, \quad \int_{\mathbb{R}} J_\rho(x)\mathrm{d}x = 1 \tag{5.34}$$

and a function $u(x)$ defined on $\mathbb{R}$ is mollified as

$$u^\rho = J_\rho * u = \int_{\mathbb{R}} J_\rho(x-y)u(y)\mathrm{d}y\,. \tag{5.35}$$

If $u(x)$ is defined only on a closed interval $[x_a, x_b]$, then it is extended as

$$u(x) = \begin{cases} u(x_a) & \text{if } x < x_a \\ u(x_b) & \text{if } x_b < x \end{cases}. \tag{5.36}$$

Assume that $\varphi_u(u)$ and $\psi_u(u)$ are continuous in the set

$$U = \left\{ u \middle| u = u_1(x) \text{ or } u = u_2(x), \exists x \in \overline{\Omega} \right\} \tag{5.37}$$

as well as in the set $\left[\min_{x\in\overline{\Omega}} \left(u_1(x), u_2(x)\right), \max_{x\in\overline{\Omega}} \left(u_1(x), u_2(x)\right) \right] \backslash U$. Then, auxiliary functions of x are defined as

$$\Phi = \int_0^1 \varphi_u\left(u_1 + \tau\left(u_2 - u_1\right)\right)\mathrm{d}\tau = \begin{cases} \dfrac{\varphi(u_1) - \varphi(u_2)}{u_1 - u_2} & \text{if } u_1 \neq u_2 \\ \varphi_u(u_1) & \text{if } u_1 = u_2 \end{cases} \tag{5.38}$$

$$\Phi_\rho = \int_0^1 \varphi_u\left(u_1^\rho + \tau\left(u_2^\rho - u_1^\rho\right)\right)\mathrm{d}\tau = \begin{cases} \dfrac{\varphi(u_1^\rho) - \varphi(u_2^\rho)}{u_1^\rho - u_2^\rho} & \text{if } u_1^\rho \neq u_2^\rho \\ \varphi_u(u_1^\rho) & \text{if } u_1^\rho = u_2^\rho \end{cases} \tag{5.39}$$

$$\Psi = \int_0^1 \psi_u \left(u_1 + \tau \left(u_2 - u_1 \right) \right) \mathrm{d}\tau = \begin{cases} \dfrac{\psi(u_1) - \psi(u_2)}{u_1 - u_2} & \text{if } u_1 \neq u_2 \\ \psi_u(u_1) & \text{if } u_1 = u_2 \end{cases} \tag{5.40}$$

and

$$\Psi_\rho = \int_0^1 \psi_u \left(u_1^\rho + \tau \left(u_2^\rho - u_1^\rho \right) \right) \mathrm{d}\tau = \begin{cases} \dfrac{\psi(u_1^\rho) - \psi(u_2^\rho)}{u_1^\rho - u_2^\rho} & \text{if } u_1^\rho \neq u_2^\rho \\ \psi_u(u_1^\rho) & \text{if } u_1^\rho = u_2^\rho \end{cases}. \tag{5.41}$$

The following lemma is the core involving the uniqueness of a GS.

Lemma 1. Assume that both of

$$\lim_{y \to x^-} \Psi(y) \lim_{y \to x^+} \Psi(y) > 0 \tag{5.42}$$

and

$$\lim_{y \to x^-} \left(\frac{\mathrm{d}\Phi(y)}{\mathrm{d}x} - \Psi(y) \right) \lim_{y \to x^+} \left(\frac{\mathrm{d}\Phi(y)}{\mathrm{d}x} - \Psi(y) \right) > 0 \tag{5.43}$$

hold for any $x \in \overline{\Omega}$ such that $\lim_{y \to x^-} \Phi(y) \lim_{y \to x^+} \Phi(y) \leq 0$. Then the linear SFO ODE

$$\Phi_\rho \frac{\mathrm{d}f}{\mathrm{d}x} = \Psi_\rho f + F \tag{5.44}$$

has a solution $f \in W^{1,1}(\Omega)$ for any $F \in C_B^1(\Omega)$ when ρ is taken small enough.

Proof. If $\lim_{y \to x^-} \Phi(y) \lim_{y \to x^+} \Phi(y) > 0$ for any $x \in \overline{\Omega}$, then there exists a constant c such that $\left| \Phi_\rho \right| \geq c > 0$ for any $x \in \overline{\Omega}$ when ρ is taken small enough. Then, an initial value problem of **(5.44)** with the initial condition $f(0) = 0$ has a solution $f \in C_B^1(\Omega) \subset W^{1,1}(\Omega)$. With the assumption of the lemma, there exists a point ξ in the ρ-neighborhood of x such that

$\Phi_\rho(\xi)=0$ and $\left|\Psi_\rho\left(\mathrm{d}\Phi_\rho/\mathrm{d}x-\Psi_\rho\right)(\xi)\right|>0$ when ρ is taken small enough. Then, solving $\Psi_\rho f+F=0$ and applying the L'Hôpital's rule to $\left(\Psi_\rho f+F\right)/\Phi_\rho$ yields

$$f=-\frac{F}{\Psi_\rho} \tag{5.45}$$

and

$$\frac{\mathrm{d}f}{\mathrm{d}x}=\frac{\Psi_\rho\dfrac{\mathrm{d}F}{\mathrm{d}x}-\dfrac{\mathrm{d}\Psi_\rho}{\mathrm{d}x}F}{\Psi_\rho\left(\dfrac{\mathrm{d}\Phi_\rho}{\mathrm{d}x}-\Psi_\rho\right)} \tag{5.46}$$

at such a ξ. If $\Phi_\rho\neq 0$ in $\left[0,x_r\right)$ and $\Phi_\rho(x_r)=0$, then an initial value problem of **(5.44)** with the initial condition $f(x_r)=-F(x_r)/\Psi_\rho(x_r)$ has a solution $f\in C_B^1(0,x_r)$. If $\Phi_\rho\neq 0$ in $\left(x_l,X\right]$ and $\Phi_\rho(x_l)=0$, then an initial value problem of **(5.44)** with the initial condition $f(x_l)=-F(x_l)/\Psi_\rho(x_l)$ has a solution $f\in C_B^1(x_l,X)$. If $\Phi_\rho\neq 0$ in $\left(x_l,x_r\right)\subset\Omega$ and $\Phi_\rho(x_l)=\Phi_\rho(x_r)=0$, then two initial value problems of **(5.44)** with the initial conditions $f(x_l)=-F(x_l)/\Psi_\rho(x_l)$ and $f(x_r)=-F(x_r)/\Psi_\rho(x_r)$ have respective solutions $f=f_l$ and $f=f_r$ in $C_B^1(x_l,x_r)$. Then, $\Delta f=f_r-f_l\in C_B^1(x_l,x_r)$ solves

$$\frac{\mathrm{d}\Delta f}{\mathrm{d}x}=\frac{\Psi_\rho}{\Phi_\rho}\Delta f \tag{5.47}$$

in $\left(x_l,x_r\right)$ with the Neumann boundary condition $\mathrm{d}\Delta f/\mathrm{d}x=0$ at $x=x_l$ and $x=x_r$, implying that $\mathrm{d}\Delta f/\mathrm{d}x=0$ and then $\Delta f=0$ in $\left(x_l,x_r\right)$. That identical

$f = f_l = f_r \in C_B^1(x_l, x_r)$ solves **(5.44)** with the Dirichlet boundary condition consisting of $f(x_l) = -F(x_l)/\Psi_\rho(x_l)$ and $f(x_r) = -F(x_r)/\Psi_\rho(x_r)$. The procedure above completes the construction of a solution $f \in C_B^1(\Omega) \subset W^{1,1}(\Omega)$ of **(5.44)**.

□

A necessary condition so that GSs are not unique is stated as follows.

Theorem 4. Suppose that there are two GSs $u_1(x)$ and $u_2(x)$ satisfying **(5.24)** for any $f \in W^{1,1}(\Omega)$. If $u_1(x)$ and $u_2(x)$ are different in the sense that there exists $F \in C_B^1(\Omega)$ such that $\int_0^X F(u_1 - u_2)\mathrm{d}x \neq 0$, then there exists $x \in \overline{\Omega}$ such that $\lim_{y \to x^-} \Phi(y) \lim_{y \to x^+} \Phi(y) \leq 0$ and either **(5.42)** or **(5.43)**, or both, does not hold.

Proof. If the assertion is false, then **Lemma 1** holds. Then,

$$\begin{aligned}
\int_0^X F(u_1 - u_2)\mathrm{d}x &= \int_0^X \left(\Phi_\rho \frac{\mathrm{d}f}{\mathrm{d}x} - \Psi_\rho f \right)(u_1 - u_2)\mathrm{d}x \\
&= \int_0^X \left((\Phi_\rho - \Phi)\frac{\mathrm{d}f}{\mathrm{d}x} - (\Psi_\rho - \Psi) f \right)(u_1 - u_2)\mathrm{d}x \\
&\quad + \int_0^X \left(\Phi \frac{\mathrm{d}f}{\mathrm{d}x} - \Psi f \right)(u_1 - u_2)\mathrm{d}x \\
&= \int_0^X \left((\Phi_\rho - \Phi)\frac{\mathrm{d}f}{\mathrm{d}x} - (\Psi_\rho - \Psi) f \right)(u_1 - u_2)\mathrm{d}x
\end{aligned} \tag{5.48}$$

because of **(5.36)**, **(5.40)**, and **(5.24)**. Let $\Delta u = u_1 - u_2$, $\Delta u^\rho = u_1^\rho - u_2^\rho$, $\Delta\varphi = \varphi(u_1) - \varphi(u_2)$, and $\Delta\varphi^\rho = \varphi(u_1^\rho) - \varphi(u_2^\rho)$. From the inequalities

$$\begin{aligned}\left|\int_0^X F\left(u_1-u_2\right)\mathrm{d}x\right| &\le \left|\int_0^X \left(\Phi_\rho-\Phi\right)\frac{\mathrm{d}f}{\mathrm{d}x}\left(u_1-u_2\right)\mathrm{d}x\right| + \left|\int_0^X \left(\Psi_\rho-\Psi\right) f\left(u_1-u_2\right)\mathrm{d}x\right| \\ &\le \left|\int_0^X \left(\Phi_\rho\left(u_1-u_2\right)-\left(\varphi(u_1)-\varphi(u_2)\right)\right)\frac{\mathrm{d}f}{\mathrm{d}x}\mathrm{d}x\right| \\ &\quad + \left\|\Psi_\rho-\Psi\right\|_{L^1}\left\|f\right\|_{L^1}\left\|u_1-u_2\right\|_{L^1}\end{aligned} \tag{5.49}$$

$$\begin{aligned}\left|\int_0^X \left(\Phi_\rho\left(u_1-u_2\right)-\left(\varphi(u_1)-\varphi(u_2)\right)\right)\frac{\mathrm{d}f}{\mathrm{d}x}\mathrm{d}x\right| &\le \left|\int_0^X \begin{pmatrix}\left(\Delta u\Phi_\rho-\Delta u^\rho\Phi_\rho\right)\frac{\mathrm{d}f}{\mathrm{d}x} \\ +\left(\Delta u^\rho\Phi_\rho-\Delta\varphi\right)\frac{\mathrm{d}f}{\mathrm{d}x}\end{pmatrix}\mathrm{d}x\right| \\ &\le \left|\int_0^X \left(\Delta u-\Delta u^\rho\right)\left(\Psi_\rho f+F\right)\mathrm{d}x\right| \\ &\quad + \left|\int_0^X \left(\left(\Delta\varphi^\rho-\Delta\varphi\right)\frac{\mathrm{d}f}{\mathrm{d}x}\right)\mathrm{d}x\right|\end{aligned} \tag{5.50}$$

and

$$\begin{aligned}\left|\int_0^X \left(\left(\Delta\varphi^\rho-\Delta\varphi\right)\frac{\mathrm{d}f}{\mathrm{d}x}\right)\mathrm{d}x\right| &\le \left|\int_0^X \begin{pmatrix}\varphi(u_1^\rho)\frac{\mathrm{d}f}{\mathrm{d}x}-\varphi(u_2^\rho)\frac{\mathrm{d}f}{\mathrm{d}x} \\ -\psi(u_1)f+\psi(u_2)f\end{pmatrix}\mathrm{d}x\right| \\ &\le \begin{vmatrix}\int_0^X \left(\varphi(u_1^\rho)\frac{\mathrm{d}f}{\mathrm{d}x}-\psi(u_1^\rho)f\right)\mathrm{d}x \\ -\int_0^X \left(\varphi(u_2^\rho)\frac{\mathrm{d}f}{\mathrm{d}x}-\psi(u_2^\rho)f\right)\mathrm{d}x\end{vmatrix} \\ &\quad + \left|\int_0^X f\left(\psi(u_1^\rho)-\psi(u_1)\right)\mathrm{d}x-\int_0^X f\left(\psi(u_2^\rho)-\psi(u_2)\right)\mathrm{d}x\right|\end{aligned} \tag{5.51}$$

,

it is concluded that $\left|\int_0^X F\left(u_1-u_2\right)\mathrm{d}x\right|$ approaches to zero for any $F\in C_B^1(\Omega)$ as passing the limit $\rho\to 0^+$, contradicting the hypothesis of $u_1\neq u_2$.

□

5.4 Illustrative examples

Numerical approximations to the solutions of **(5.26)** for several different cases illustrate characteristics of the 1D steady open channel flows. The acceleration due to gravity, the roughness coefficient, and the exponent are fixed as $g = 9.80665$, $n = 0.01$, and $p = 2/3$, respectively. Firstly, we consider rectangular cross-sectional channels with different slopes to revisit the conventional classification of flows in open channel hydraulics. Then, we address the non-uniqueness of solutions in a modified circular cross-sectional channel.

5.4.1 Unique solutions in rectangular cross-sectional channels

The constant width of the rectangular cross-sectional channels is set as $\partial A/\partial h = 0.6$. The discharge is given as $Q = 0.01$. Then, the value of the critical flow depth is in the range $0.0304830 < h_{\text{cri}} < 0.0304831$. There is a single uniform flow depth h_{uni} if the bed slope S_0 is positive, whereas a real h_{uni} does not exist if $S_0 \le 0$. The value of the bed slope $S_0 = S_{\text{cri}}$ achieving $h_{\text{uni}} = h_{\text{cri}}$ is in the range $1/139.991 < S_{\text{cri}} < 1/139.990$. Channels with $S_0 > S_{\text{cri}}$, $S_0 = S_{\text{cri}}$, $0 < S_0 < S_{\text{cri}}$, $S_0 = 0$, and $S_0 < 0$ are referred to as the steep slope channel, the critical slope channel, the mild slope channel, the horizontal slope channel, and the adverse slope channel, respectively. **Figure 5.2**- **Figure 5.6** show the computed water surface profiles of the GVFSs for different slopes, with appropriate Galilean transformations, for the channels of $S_0 = 2S_{\text{cri}}$, $S_0 = S_{\text{cri}}$, $S_0 = S_{\text{cri}}/2$, $S_0 = 0$, and $S_0 = -S_{\text{cri}}$. According to the conventional classification of flows in open channel hydraulics, the GVFSs as per **Remark 1** are labeled

as S1, S2, etc. The GVFSs as per **Remark 2** are the uniform flow depths (lines in blue color) appearing in the steep, the critical, and the mild slope channels. In the critical slope channel, **Remark 4** is indeed the case. As per **Theorem 3**, a hydraulic jump between two different GVFSs across the critical flow depth occurs if and only if an appropriate Galilean transformation is applied to one of the GVFSs so that the specific forces $F_s = -\varphi$ (represented as different colors) coincide at a point ξ.

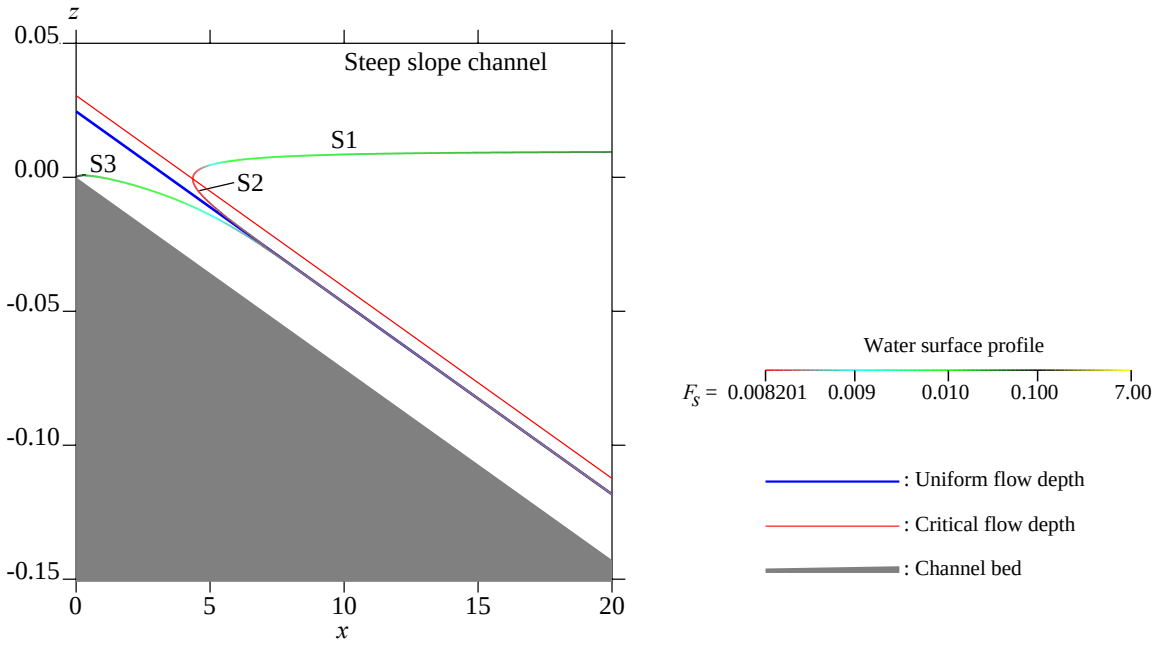

Figure 5.2. GVFSs in rectangular cross-sectional channels of steep slope channel.

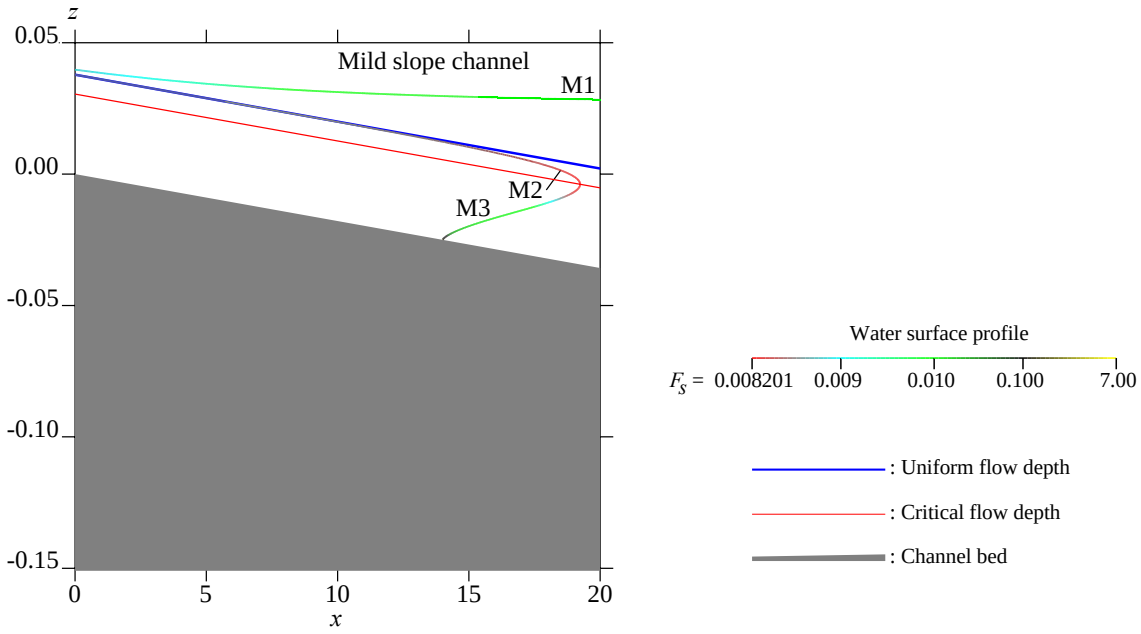

Figure 5.3. GVFSs in rectangular cross-sectional channels of mild slope channel.

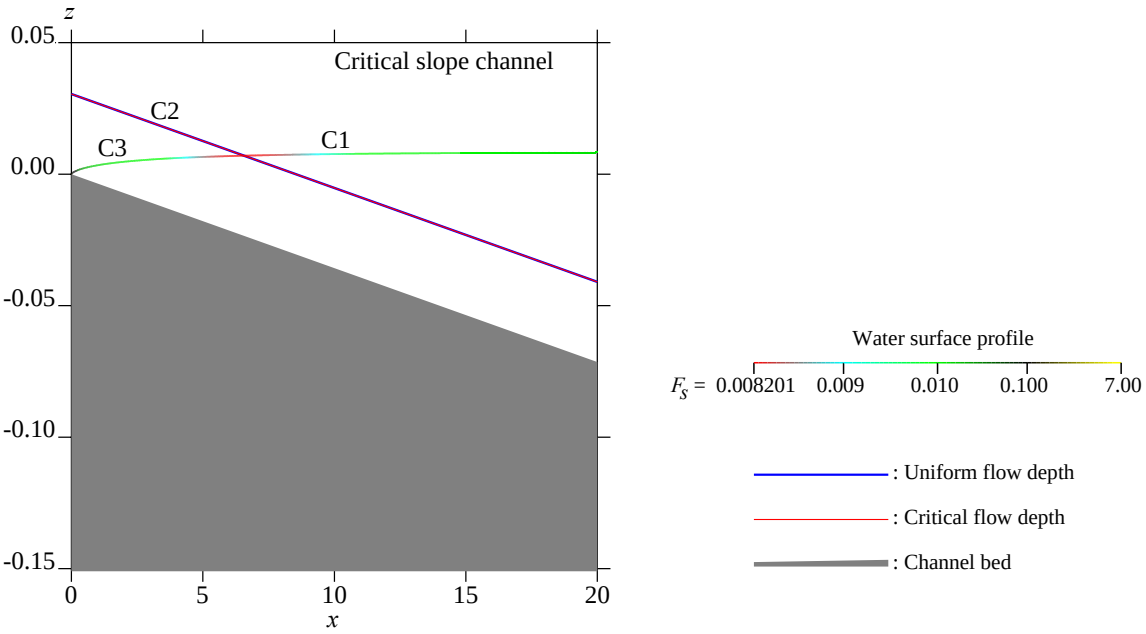

Figure 5.4. GVFSs in rectangular cross-sectional channels of critical slope channel.

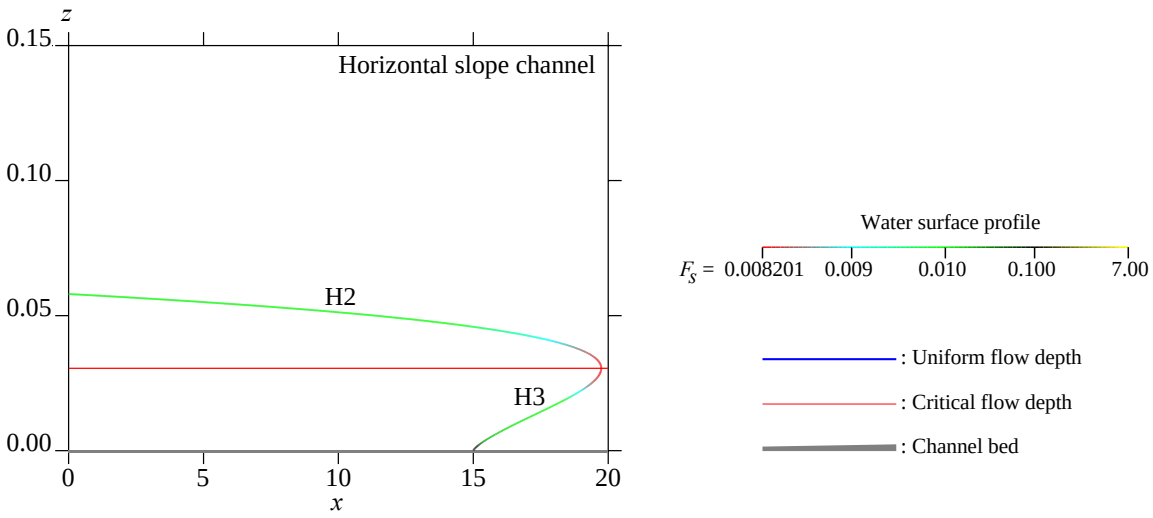

Figure 5.5. GVFSs in rectangular cross-sectional channels of horizontal slope channel.

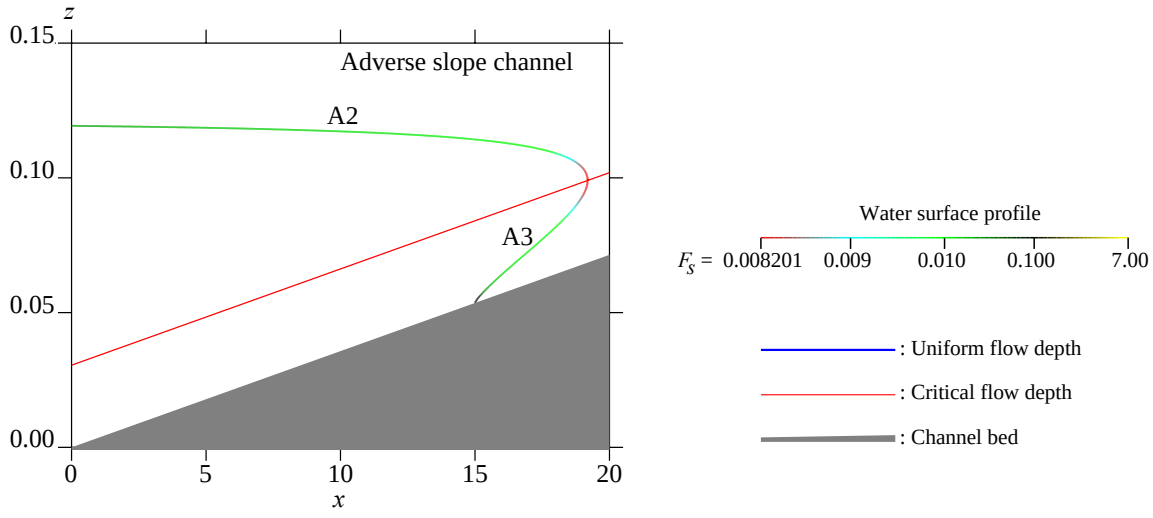

Figure 5.6. GVFSs in rectangular cross-sectional channels of adverse slope channel.

5.4.2 Non-unique solutions in a modified circular cross-sectional channel

There are non-unique VSs of a Dirichlet problem, and thus GSs, in the channel having a modified circular cross-section whose shape is shown in the top-left of **Figure 5.7**; the top part of the circle with a diameter 0.10 above $z = z_{\mathrm{cri}}$ is replaced with the symmetric two chords. The discharge Q, the bed slope S_0, and the height z_{cri} of the chords' feet are set so that there is a single uniform depth h_{uni} achieving $h_{\mathrm{uni}} = h_{\mathrm{cri}} = z_{\mathrm{cri}}$ under the fixed conditions of the other parameters. The resulting values are estimated as $0.00955282 < Q < 0.00955283$, $1/57.1774 < S_0 < 1/57.1773$, and $0.0938181 < z_{\mathrm{cri}} < 0.0938182$. Note that there can be two uniform depths in general in a circular cross-sectional channel.

The Dirichlet problem consists of the governing equation **(5.21)** in the viscosity sense, the specified downstream endpoint $X = 10$, and the Dirichlet boundary condition **(5.23)** with the specified boundary values $u_{\mathrm{up}} = \log 0.08$ and $u_{\mathrm{down}} = u_{\mathrm{uni}} = u_{\mathrm{cri}}$. As $\varphi_u(u_{\mathrm{up}}) > 0$ and $\varphi_u(u_{\mathrm{down}}) = 0$, a VS can exist according to **Theorem 2**. Indeed, there is an S3-like GVFS below $u_{\mathrm{uni}} = u_{\mathrm{cri}}$ satisfying the upstream boundary condition. There is an infinite number of VSs in $C_B(\Omega)$ above or at $u_{\mathrm{uni}} = u_{\mathrm{cri}}$ satisfying the downstream boundary condition as mentioned in **Remark 4** with non-smoothness at arbitrary $\xi \in \overline{\Omega}$. Therefore, there is an infinite number of VSs of the Dirichlet problem, having a discontinuity across $u_{\mathrm{uni}} = u_{\mathrm{cri}}$ at an arbitrary point in a certain range in Ω. Here, as plotted in the top-right of **Figure 5.7**, we choose two VSs $u_1(x)$ (thick lines) and $u_2(x)$ (thin lines) having discontinuities at $x = \xi_1 = 4$ and at $x = \xi_2 = 7$, respectively. The non-smooth points of $u_1(x)$ and $u_2(x)$ in the $C_B(\Omega)$

parts are close to $x = 5.90$ and $x = 8.02$, respectively. The auxiliary functions Φ (in red color), Ψ (in green color), and $\Phi_x - \Psi = \mathrm{d}\Phi/\mathrm{d}x - \Psi$ (in blue color), are plotted in the bottom-right of **Figure 5.7**. Spurious oscillations in $\Phi_x - \Psi$ around the non-smooth points of the VSs are due to numerical differentiation of Φ. The points $x \in \overline{\Omega}$ such that $\lim_{y \to x^-} \Phi(y) \lim_{y \to x^+} \Phi(y) \leq 0$ are $x = \xi_1 = 4$ and $x = \xi_2 = 7$. At each of those points x, both of **(5.42)** and **(5.43)** are violated, and thus the assertion of **Theorem 4** is confirmed.

Lastly, we address the stability of the VSs. The S3-like GVFS below $u_{\mathrm{uni}} = u_{\mathrm{cri}}$ with the upstream boundary condition $u_{\mathrm{up}} = \log 0.08$ satisfies a downstream boundary condition $u_{\mathrm{down}} = \log h_X$, where $0.0924501 < h_X < 0.0924640 < z_{\mathrm{cri}}$. Therefore, the Dirichlet boundary problem changing u_{down} from u_{cri} to $u_{\mathrm{cri}} - \varepsilon$ with sufficiently small positive constant ε does not have any solution, implying the instability of the VSs of the original Dirichlet problem.

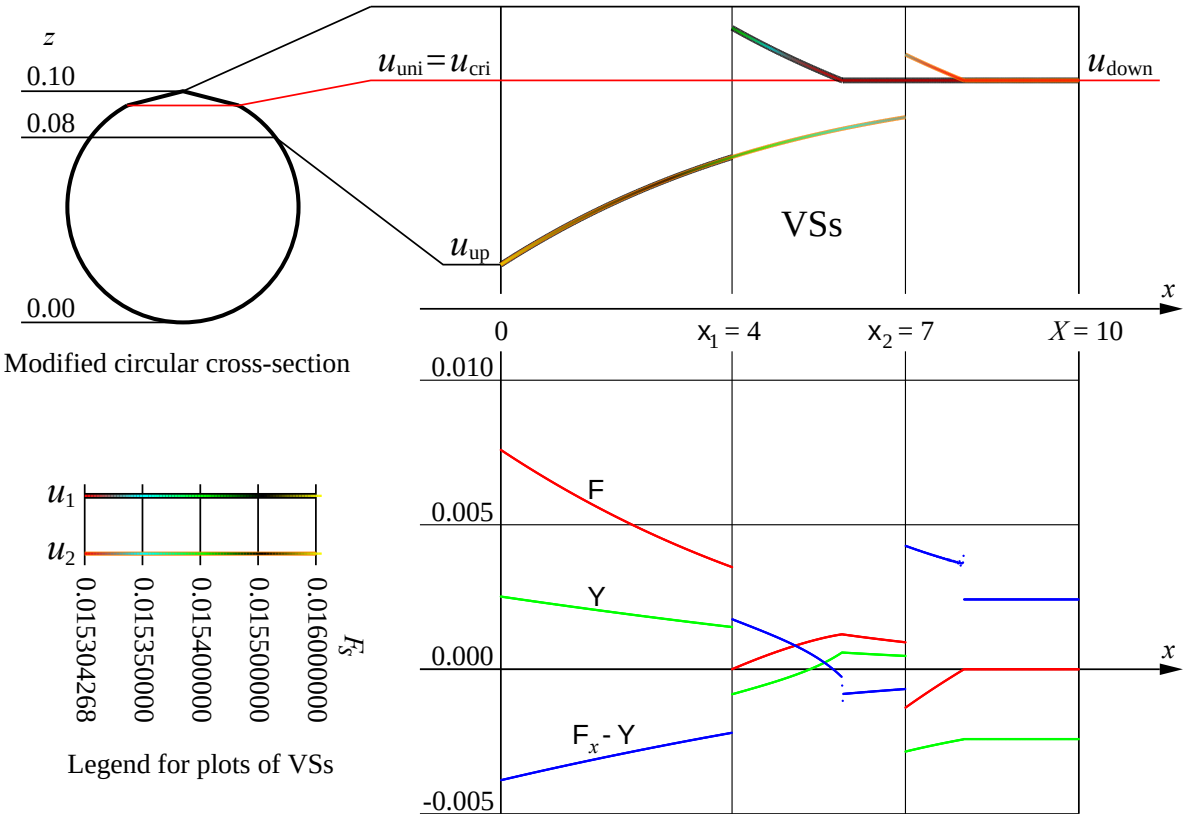

Figure 5.7. Non-unique VSs of the Dirichlet problem in the modified circular cross-sectional channel with the auxiliary functions.

5.5 Conclusions

This chapter has presented a thorough description of 1D steady open channel flows, whose water surface profiles are represented by the VSs of the Dirichlet problems in a bounded open x-domain Ω. The governing HJ equation is FOQL with an improper Hamiltonian function. The VSs include the GVFSs and the hydraulic jumps satisfying the entropy condition, which have been known in conventional open channel hydraulics. The U-

env and the L-env of a VS belong to $USC\left(\overline{\Omega}\right)$ and $LSC\left(\overline{\Omega}\right)$, respectively, but the VS is identical with a GS in the space $L^1(\Omega)\cap L^\infty(\Omega)$. The non-uniqueness of GSs and thus of VSs involving discontinuities depends on the regularity of the Hamiltonian function, determined by the channel's cross-sectional shape. The necessary condition of non-uniqueness is described in terms of the auxiliary functions. The illustrative examples include the unique solutions in the rectangular cross-sectional and non-unique solutions in the modified circular cross-sectional channel. The implication of non-uniqueness shall be researched for further understanding of 1D open channel flows.

Chapter 6

6 Summation

6.1 Conclusions

This thesis described the mathematical and numerical modeling of open channel flows locally 1D, addressing dry bed and discontinuities of water surface profiles. The results from each chapter can be summarized as follows.

In Chapter 3, level-set methods applying to the kinematic wave equation governing surface water flows have been discussed. The methods deal with the critical issues arising from the governing nonlinear equations in surface water hydrodynamic included discontinuities in water surface levels and treatment of dry beds or zero water depths. The development of overturning has been regulated with SVR, whose effect is to improve the zeros of the level-set function moving closer to the exact solutions of the shock fronts in dam-break problems. The method has been primarily verified with the explicitly known exact

positions of primitive dam-break problems, optimizing a parameter of SVR. Then, the computation of the sudden water release from Chan Thnal Reservoir, Kampong Speu Province, Cambodia, into its irrigation canal system with the initially dry bed has been simulated as a practical demonstrative example. The proposed method produces the results with free spurious diffusive deformation of water surfaces even if a relatively coarse computational mesh is used. However, the model induced a non-realistic flow propagation downstream. It restricted the flow to remain constant as upstream water depth due to the treatment of the kinematic wave equation as the Hamilton-Jacobi type. To deal with this problem, we considered another method to yield more realistic flow profiles of the dry bed in Chapter 4.

In Chapter 4, the kinematic wave model under the assumption of balanced gravity and friction forces has been applied in open channel hydraulics and surface hydrology. There persists a misunderstanding that a discontinuity of a kinematic wave occurs due to a discontinuity of input and then dissipates. The study of this chapter has clarified that a discontinuity can develop without dissipation under the smoothness of all input and has provided the numerical solutions of the kinematic wave equation over the dry bed with the varied bed slopes that the case was not successfully treated in Chapter 3. The FOQL PDEs theory shows that Cauchy problems for the kinematic wave model have unique measurable and bounded solutions, which are possibly discontinuous. Numerical examples of Case 1 dealing with the practical problem of Chan Thnal Reservoir's irrigational canal system with non-smooth initial data and Case 2 addressing the hypothetical problem with smooth initial data have been demonstrated to visualize the fundamental properties of the discontinuous kinematic waves and the non-dissipative shock waves. Both numerical examples have been

computed with the initial dry bed. Nevertheless, the model is limited to input precisely zero initial condition. Instead, we used a sufficiently small initial condition considered the dry bed case in most literature.

In Chapter 5, it determines water surface profiles of steady open channel flows in a one-dimensional bounded domain Ω, which is one of the well-trodden topics in conventional hydraulic engineering. The advantages of using the notion of VS to thoroughly describe the characteristics of possibly GSs to Dirichlet problems of scalar first-order quasilinear ordinary differential equations, which are of mathematical interest, have been proven in mathematical aspects. Those VSs are the GSs in the space $L^1(\Omega) \cap L^\infty(\Omega)$. The GSs to some Dirichlet problems are not always unique, and a necessary condition for the non-uniqueness has been derived. A concrete example illustrates the non-uniqueness of discontinuous VSs in a modified circular cross-sectional shape channel. The significant results of this chapter could provide a better understanding of the ill-posed problem for the scalar first-order quasilinear ordinary differential equations with Dirichlet boundary conditions.

6.2 Future works

In the future, the mathematical and numerical modeling will be proved and improved to apply in various hydro-environmental problems with the GSs over the dry bed. The follow-up studies are summarized below

- The level-set method for the kinematic wave equation with the dry bed case shall be improved to produce a more realistic flow propagation downstream. Then, we shall

extend the technique to the full dynamics SWEs to treat more irregular topography, roughness, lateral flows, and channel junctions.

- The rigorous mathematical analysis shall be proven in a future study to provide concrete evidence of the discontinuities.
- Further studies on the implication of non-uniqueness shall be researched for 1D open channel flows.

References

[1] R. Szymkiewicz, *Numerical modeling in open channel hydraulics*. Springer, 2010.

[2] S. Bunya, E. J. Kubatko, J. J. Westerink, and C. Dawson, "A wetting and drying treatment for the Runge–Kutta discontinuous Galerkin solution to the shallow water equations," *Comput. Methods Appl. Mech. Eng.*, vol. 198, no. 17–20, pp. 1548–1562, 2009.

[3] G. Hernandez-Duenas and A. Beljadid, "A central-upwind scheme with artificial viscosity for shallow-water flows in channels," *Adv. Water Resour.*, vol. 96, pp. 323–338, 2016.

[4] X. Ying and S. S. Y. Wang, "Improved implementation of the HLL approximate Riemann solver for one-dimensional open channel flows," *J. Hydraul. Res.*, vol. 46, no. 1, pp. 21–34, 2008.

[5] V. P. Singh, "Kinematic Wave Theory of Overland Flow," *Water Resour. Manag.*, vol. 31, no. 10, pp. 3147–3160, 2017, doi: 10.1007/s11269-017-1654-1.

[6] R. Misra, K. Sridharan, and M. S. Mohan Kumar, "Transients in Canal Network," *J. Irrig. Drain. Eng.*, vol. 118, no. 5, pp. 690–707, Sep. 1992, doi: 10.1061/(ASCE)0733-9437(1992)118:5(690).

[7] H. W. J. Kernkamp, A. Van Dam, G. S. Stelling, and E. D. de Goede, "Efficient

scheme for the shallow water equations on unstructured grids with application to the Continental Shelf," *Ocean Dyn.*, vol. 61, no. 8, pp. 1175–1188, 2011.

[8] G. Kesserwani and Q. Liang, "Well-balanced RKDG2 solutions to the shallow water equations over irregular domains with wetting and drying," *Comput. Fluids*, vol. 39, no. 10, pp. 2040–2050, 2010, doi: https://doi.org/10.1016/j.compfluid.2010.07.008.

[9] J. Burguete, P. García-Navarro, and J. Murillo, "Friction term discretization and limitation to preserve stability and conservation in the 1D shallow-water model: Application to unsteady irrigation and river flow," *Int. J. Numer. Methods Fluids*, vol. 58, no. 4, pp. 403–425, 2008.

[10] Z. Cao, G. Pender, S. Wallis, and P. Carling, "Computational dam-break hydraulics over erodible sediment bed," *J. Hydraul. Eng.*, vol. 130, no. 7, pp. 689–703, 2004.

[11] S. Fomel, S. Luo, and H. Zhao, "Fast sweeping method for the factored eikonal equation," *J. Comput. Phys.*, vol. 228, no. 17, pp. 6440–6455, Sep. 2009, doi: 10.1016/j.jcp.2009.05.029.

[12] H. M. Kalita, "A Numerical Model for 1D Bed Morphology Calculations," *Water Resour. Manag.*, vol. 34, no. 15, pp. 4975–4989, 2020.

[13] S. Leakey, C. J. M. Hewett, V. Glenis, and P. F. Quinn, "Modelling the Impact of Leaky Barriers with a 1D Godunov-Type Scheme for the Shallow Water Equations," *Water*, vol. 12, no. 2, p. 371, 2020.

[14] X. Lai, Q. Huang, Y. Zhang, and J. Jiang, "Impact of lake inflow and the Yangtze River flow alterations on water levels in Poyang Lake, China," *Lake Reserv. Manag.*, vol. 30, no. 4, pp. 321–330, 2014.

[15] S. Tinti and R. Tonini, "Analytical evolution of tsunamis induced by near-shore

earthquakes on a constant-slope ocean," *J. Fluid Mech.*, vol. 535, p. 33, 2005.

[16] K. Kobayashi and K. Takara, "Development of a distributed rainfall-run-off/flood-inundation simulation and economic risk assessment model," *J. Flood Risk Manag.*, vol. 6, no. 2, pp. 85–98, 2013.

[17] M. J. Lighthill and G. B. Whitham, "On kinematic waves I. Flood movement in long rivers," *Proc. R. Soc. London. Ser. A. Math. Phys. Sci.*, vol. 229, no. 1178, pp. 281–316, May 1955, doi: 10.1098/rspa.1955.0088.

[18] V. P. Singh and J. L. M. P. de Lima, "One-dimensional linear kinematic wave solution for overland flow under moving storms using the method of characteristics," *J. Hydrol. Eng.*, vol. 23, no. 7, p. 4018029, 2018.

[19] T. Y. K. Chen and H. Capart, "Kinematic wave solutions for dam-break floods in non-uniform valleys," *J. Hydrol.*, vol. 582, p. 124381, 2020.

[20] Q. Q. Liu and V. P. Singh, "Effect of microtopography, slope length and gradient, and vegetative cover on overland flow through simulation," *J. Hydrol. Eng.*, vol. 9, no. 5, pp. 375–382, 2004.

[21] Q. Ran, D. Su, P. Li, and Z. He, "Experimental study of the impact of rainfall characteristics on runoff generation and soil erosion," *J. Hydrol.*, vol. 424, pp. 99–111, 2012.

[22] D. A. Howes, A. D. Abrahams, and E. B. Pitman, "One-and two-dimensional modelling of overland flow in semiarid shrubland, Jornada basin, New Mexico," *Hydrol. Process. An Int. J.*, vol. 20, no. 5, pp. 1027–1046, 2006.

[23] J. M. G. P. Isidoro and J. L. M. P. de Lima, "Analytical closed-form solution for 1D linear kinematic overland flow under moving rainstorms," *J. Hydrol. Eng.*, vol. 18, no.

9, pp. 1148–1156, 2013.

[24] W. L. Jin, “A kinematic wave theory of lane-changing traffic flow,” *Transp. Res. part B Methodol.*, vol. 44, no. 8–9, pp. 1001–1021, 2010.

[25] B. Mukhopadhyay, J. Cornelius, and W. Zehner, “Application of kinematic wave theory for predicting flash flood hazards on coupled alluvial fan–piedmont plain landforms,” *Hydrol. Process.*, vol. 17, no. 4, pp. 839–868, 2003.

[26] E. Han and G. Warnecke, “Exact Riemann solutions to shallow water equations,” *Q. Appl. Math.*, vol. 72, no. 3, pp. 407–453, 2014.

[27] N. A. Alias, Q. Liang, and G. Kesserwani, “A Godunov-type scheme for modelling 1D channel flow with varying width and topography,” *Comput. Fluids*, vol. 46, no. 1, pp. 88–93, 2011, doi: https://doi.org/10.1016/j.compfluid.2010.12.009.

[28] A. Ern, S. Piperno, and K. Djadel, “A well-balanced Runge–Kutta discontinuous Galerkin method for the shallow-water equations with flooding and drying,” *Int. J. Numer. methods fluids*, vol. 58, no. 1, pp. 1–25, 2008.

[29] M. Zijlema, “The role of the Rankine-Hugoniot relations in staggered finite difference schemes for the shallow water equations,” *Comput. Fluids*, vol. 192, p. 104274, 2019, doi: https://doi.org/10.1016/j.compfluid.2019.104274.

[30] K. Yokoi and F. Xiao, “Mechanism of structure formation in circular hydraulic jumps: numerical studies of strongly deformed free-surface shallow flows,” *Phys. D Nonlinear Phenom.*, vol. 161, no. 3, pp. 202–219, 2002, doi: https://doi.org/10.1016/S0167-2789(01)00370-0.

[31] V. Te Chow, *Open-channel Hydraulics: International Student Ed*. New York, 1959.

[32] A. M. Gharangik and M. H. Chaudhry, “Numerical Simulation of Hydraulic Jump,” *J. Hydraul. Eng.*, vol. 117, no. 9, pp. 1195–1211, Sep. 1991, doi: 10.1061/(ASCE)0733-9429(1991)117:9(1195).

[33] J. M. Carrillo, F. Marco, L. G. Castillo, and J. T. García, “Experimental study of submerged hydraulic jumps generated downstream of rectangular plunging jets,” *Int. J. Multiph. Flow*, vol. 137, p. 103579, 2021.

[34] S. Harada and S. S. Li, “Modelling hydraulic jump using the bubbly two-phase flow method,” *Environ. Fluid Mech.*, vol. 18, no. 2, pp. 335–356, 2018.

[35] P. L. Lions, *Generalized solutions of Hamilton-Jacobi equations*. Pitman, 1982.

[36] H. Ishii and P. L. Lions, “Viscosity solutions of fully nonlinear second-order elliptic partial differential equations,” *J. Differ. Equ.*, vol. 83, no. 1, pp. 26–78, 1990, doi: https://doi.org/10.1016/0022-0396(90)90068-Z.

[37] M. G. Crandall and P. L. Lions, “Viscosity solutions of Hamilton-Jacobi equations,” *Trans. Am. Math. Soc.*, vol. 277, no. 1, pp. 1–42, Jan. 1983, doi: 10.1090/s0002-9947-1983-0690039-8.

[38] M. G. Crandall, H. Ishii, and P. L. Lions, “User’s guide to viscosity solutions of second order partial differential equations,” *Bull. Am. Math. Soc.*, vol. 27, no. 1, pp. 1–67, 1992, doi: 10.1090/S0273-0979-1992-00266-5.

[39] Y. Achdou, G. Barles, H. Ishii, and G. L. Litvinov, “Hamilton-Jacobi equations: approximations, numerical analysis and applications,” 2013.

[40] M. Bardi and I. Capuzzo-Dolcetta, *Optimal control and viscosity solutions of Hamilton-Jacobi-Bellman equations*. Springer Science & Business Media, 2008.

[41] M. Bardi and I. Capuzzo-Dolcetta, *Optimal Control and Viscosity Solutions of Hamilton-Jacobi-Bellman Equations*. Boston: Birkhäuser Boston, 1997.

[42] G. Q. Chen and B. Su, "Discontinuous solutions of Hamilton-Jacobi equations: Existence, uniqueness, and regularity," in *Hyperbolic Problems: Theory, Numerics, Applications*, Springer, 2003, pp. 443–453.

[43] G. Barles, "Discontinuous viscosity solutions of first-order Hamilton-Jacobi equations: a guided visit," *Nonlinear Anal. Theory, Methods Appl.*, vol. 20, no. 9, pp. 1123–1134, 1993, doi: https://doi.org/10.1016/0362-546X(93)90098-D.

[44] M. Bardi and Y. Giga, "Right accessibility of semicontinuous initial data for Hamilton-Jacobi equations," *Hokkaido Univ. Prepr. Ser. Math.*, vol. 605, pp. 1–16, 2003.

[45] G. Barles and B. Perthame, "Discontinuous solutions of deterministic optimal stopping time problems," *ESAIM M2AN*, vol. 21, no. 4, pp. 557–579, 1987, [Online]. Available: https://doi.org/10.1051/m2an/1987210405571.

[46] E. N. Barron and R. Jensen, "Semicontinuous viscosity solutions for Hamilton–Jacobi equations with convex Hamiltonians," *Commun. Partial Differ. Equations*, vol. 15, no. 12, pp. 293–309, 1990.

[47] G. Q. Chen and B. Su, "On global discontinuous solutions of Hamilton–Jacobi equations," *Comptes Rendus Math.*, vol. 334, no. 2, pp. 113–118, 2002, doi: https://doi.org/10.1016/S1631-073X(02)02228-8.

[48] Y. Giga and M. H. Sato, "A level set approach to semicontinuous viscosity solutions for Cauchy problems," *Commun. Partial Differ. Equations*, vol. 26, no. 5–6, pp. 813–839, 2001.

[49] A. I. Subbotin, *Generalized solutions of first order PDEs: the dynamical optimization perspective*. Springer Science & Business Media, 2013.

[50] X. Chen and B. Liu, "Existence and uniqueness theorem for uncertain differential equations," *Fuzzy Optim. Decis. Mak.*, vol. 9, no. 1, pp. 69–81, 2010, doi: 10.1007/s10700-010-9073-2.

[51] H. Ishii, "Hamilton-Jacobi equations with discontinuous Hamiltonians on arbitrary open sets," *Bull. Fac. Sci. Eng. Chuo Univ*, vol. 28, no. 28, p. 1985, 1985.

[52] H. Ishii, "Perron's method for Hamilton-Jacobi equations," *Duke Math. J.*, vol. 55, no. 2, pp. 369–384, 1987, doi: 10.1215/S0012-7094-87-05521-9.

[53] M. Bertsch, F. Smarrazzo, A. Terracina, and A. Tesei, "Discontinuous viscosity solutions of first order Hamilton-Jacobi equations," *arXiv Prepr. arXiv1906.05625*, 2019.

[54] G. Barles, "Existence results for first order Hamilton Jacobi equations," *Ann. l'Institut Henri Poincare Non Linear Anal.*, vol. 1, no. 5, pp. 325–340, 1984, doi: https://doi.org/10.1016/S0294-1449(16)30415-2.

[55] H. Frankowska, "Hamilton-Jacobi equations: Viscosity solutions and generalized gradients," *J. Math. Anal. Appl.*, vol. 141, no. 1, pp. 21–26, 1989, doi: https://doi.org/10.1016/0022-247X(89)90203-5.

[56] S. Mean, K. Unami, and M. Fujihara, "Level-set methods applied to the kinematic wave equation governing surface water flows," *J. Environ. Manage.*, vol. 269, p. 110784, 2020, doi: https://doi.org/10.1016/j.jenvman.2020.110784.

[57] A. A. Khan, "Modeling flow over an initially dry bed," *J. Hydraul. Res.*, vol. 38, no. 5, pp. 383–388, Sep. 2000, doi: 10.1080/00221680009498319.

[58] X. Álvarez, M. Gómez-Rúa, and J. Vidal-Puga, “River flooding risk prevention: A cooperative game theory approach,” *J. Environ. Manage.*, vol. 248, p. 109284, Oct. 2019, doi: 10.1016/j.jenvman.2019.109284.

[59] O. Castro-Orgaz and H. Chanson, “Ritter’s dry-bed dam-break flows: positive and negative wave dynamics,” *Environ. Fluid Mech.*, vol. 17, no. 4, pp. 665–694, Aug. 2017, doi: 10.1007/s10652-017-9512-5.

[60] R. Berndtsson *et al.*, “Drivers of changing urban flood risk: A framework for action,” *J. Environ. Manage.*, vol. 240, pp. 47–56, Jun. 2019, doi: 10.1016/j.jenvman.2019.03.094.

[61] M. P. Mohanty, H. Vittal, V. Yadav, S. Ghosh, G. S. Rao, and S. Karmakar, “A new bivariate risk classifier for flood management considering hazard and socio-economic dimensions,” *J. Environ. Manage.*, vol. 255, p. 109733, Feb. 2020, doi: 10.1016/j.jenvman.2019.109733.

[62] Y. A. Abebe, A. Ghorbani, I. Nikolic, Z. Vojinovic, and A. Sanchez, “Flood risk management in Sint Maarten – A coupled agent-based and flood modelling method,” *J. Environ. Manage.*, vol. 248, p. 109317, Oct. 2019, doi: 10.1016/j.jenvman.2019.109317.

[63] K. Unami and A. H. M. B. Alam, “Concurrent use of finite element and finite volume methods for shallow water flows in locally 1D channel networks,” *Int. J. Numer. Methods Fluids*, vol. 69, no. 2, pp. 255–272, 2012, doi: 10.1002/fld.2554.

[64] N. Gouta and F. Maurel, “A finite volume solver for 1D shallow-water equations applied to an actual river,” *Int. J. Numer. Methods Fluids*, vol. 38, no. 1, pp. 1–19, Jan. 2002, doi: 10.1002/fld.201.

[65] J. P. Vila, F. Chazel, and P. Noble, “2D Versus 1D Models for Shallow Water

Equations," *Procedia IUTAM*, vol. 20, pp. 167–174, Jan. 2017, doi: 10.1016/J.PIUTAM.2017.03.023.

[66] J. J. Stoker, *Water waves: The mathematical theory with applications*. John Wiley & Sons, 1957.

[67] R. J. LeVeque, "Balancing Source Terms and Flux Gradients in High-Resolution Godunov Methods: The Quasi-Steady Wave-Propagation Algorithm," *J. Comput. Phys.*, vol. 146, no. 1, pp. 346–365, Oct. 1998, doi: 10.1006/JCPH.1998.6058.

[68] Q. Liang and F. Marche, "Numerical resolution of well-balanced shallow water equations with complex source terms," *Adv. Water Resour.*, vol. 32, no. 6, pp. 873–884, Jun. 2009, doi: 10.1016/J.ADVWATRES.2009.02.010.

[69] J. Murillo, P. García-Navarro, J. Burguete, and P. Brufau, "The influence of source terms on stability, accuracy and conservation in two-dimensional shallow flow simulation using triangular finite volumes," *Int. J. Numer. Methods Fluids*, vol. 54, no. 5, pp. 543–590, Jun. 2007, doi: 10.1002/fld.1417.

[70] M. E. Vázquez-Cendón, "Improved Treatment of Source Terms in Upwind Schemes for the Shallow Water Equations in Channels with Irregular Geometry," *J. Comput. Phys.*, vol. 148, no. 2, pp. 497–526, Jan. 1999, doi: 10.1006/jcph.1998.6127.

[71] J. Hou *et al.*, "An implicit friction source term treatment for overland flow simulation using shallow water flow model," *J. Hydrol.*, vol. 564, pp. 357–366, Sep. 2018, doi: 10.1016/J.JHYDROL.2018.07.027.

[72] Y. Liu, Y. Shi, D. A. Yuen, E. O. D. Sevre, X. Yuan, and H. L. Xing, "Comparison of linear and nonlinear shallow wave water equations applied to tsunami waves over the China Sea," *Acta Geotech.*, vol. 4, no. 2, pp. 129–137, Jun. 2009, doi: 10.1007/s11440-008-0073-0.

[73] Z. N. Zhu, X. H. Zhu, and X. Guo, “Coastal tomographic mapping of nonlinear tidal currents and residual currents,” *Cont. Shelf Res.*, vol. 143, pp. 219–227, Jul. 2017, doi: 10.1016/j.csr.2016.06.014.

[74] M. Akbar and S. Aliabadi, “Hybrid numerical methods to solve shallow water equations for hurricane induced storm surge modeling,” *Environ. Model. Softw.*, vol. 46, pp. 118–128, Aug. 2013, doi: 10.1016/j.envsoft.2013.03.003.

[75] L. Cozzolino, L. Cimorelli, R. Della Morte, G. Pugliano, V. Piscopo, and D. Pianese, “Flood propagation modeling with the Local Inertia Approximation: Theoretical and numerical analysis of its physical limitations,” *Adv. Water Resour.*, vol. 133, Nov. 2019, doi: 10.1016/j.advwatres.2019.103422.

[76] P. D. Bates, M. S. Horritt, and T. J. Fewtrell, “A simple inertial formulation of the shallow water equations for efficient two-dimensional flood inundation modelling,” *J. Hydrol.*, vol. 387, no. 1–2, pp. 33–45, Jun. 2010, doi: 10.1016/j.jhydrol.2010.03.027.

[77] E. Audusse and M. O. Bristeau, “Transport of pollutant in shallow water a two time steps kinetic method,” *ESAIM Math. Model. Numer. Anal.*, vol. 37, no. 2, pp. 389–416, 2003, doi: 10.1051/m2an:2003034.

[78] A. Kuriqi and M. Ardiçlioğlu, “Investigation of hydraulic regime at middle part of the Loire River in context of floods and low flow events,” *Pollack Period.*, vol. 13, no. 1, pp. 145–156, 2018.

[79] M. Ardıçlıoğlu and A. Kuriqi, “Calibration of channel roughness in intermittent rivers using HEC-RAS model: Case of Sarimsakli creek, Turkey,” *SN Appl. Sci.*, vol. 1, no. 9, pp. 1–9, 2019.

[80] J. E. Miller, “Basic concepts of kinematic-wave models,” 1984. doi: 10.3133/PP1302.

[81] V. P. Singh, “Kinematic wave modelling in water resources: a historical perspective,” *Hydrol. Process.*, vol. 15, no. 4, pp. 671–706, Mar. 2001, doi: 10.1002/hyp.99.

[82] H. Bao, L. Wang, K. Zhang, and Z. Li, “Application of a developed distributed hydrological model based on the mixed runoff generation model and 2D kinematic wave flow routing model for better flood forecasting,” *Atmos. Sci. Lett.*, vol. 18, no. 7, pp. 284–293, Jul. 2017, doi: 10.1002/asl.754.

[83] H. Jin-bai, W. Jia-wei, W. Bin, and Z. Shi-jiang, “Numerical analysis of the combined rainfall-runoff process and snowmelt for the Alun River Basin, Heilongjiang, China,” *Environ. Earth Sci.*, vol. 74, no. 9, pp. 6929–6941, Nov. 2015, doi: 10.1007/s12665-015-4694-y.

[84] A. Yomoto and M. N. Islam, “Kinematic analysis of flood runoff for a small-scale upland field,” *J. Hydrol.*, vol. 137, no. 1–4, pp. 311–326, Aug. 1992, doi: 10.1016/0022-1694(92)90062-Z.

[85] V. Caselles, F. Catté, T. Coll, and F. Dibos, “A geometric model for active contours in image processing,” *Numer. Math.*, vol. 66, no. 1, pp. 1–31, Dec. 1993, doi: 10.1007/BF01385685.

[86] S. Osher and J. A. Sethian, “Fronts propagating with curvature-dependent speed: Algorithms based on Hamilton-Jacobi formulations,” *J. Comput. Phys.*, vol. 79, no. 1, pp. 12–49, Nov. 1988, doi: 10.1016/0021-9991(88)90002-2.

[87] F. Gibou, R. Fedkiw, and S. Osher, “A review of level-set methods and some recent applications,” *J. Comput. Phys.*, vol. 353, pp. 82–109, Jan. 2018, doi: 10.1016/J.JCP.2017.10.006.

[88] C. Li, C. Xu, C. Gui, and M. D. Fox, “Distance regularized level set evolution and its application to image segmentation,” *IEEE Trans. Image Process.*, vol. 19, no. 12, pp.

3243–3254, Dec. 2010, doi: 10.1109/TIP.2010.2069690.

[89] R. Malladi, J. A. Sethian, and B. C. Vemuri, “Shape Modeling with Front Propagation: A Level Set Approach,” *IEEE Trans. Pattern Anal. Mach. Intell.*, vol. 17, no. 2, pp. 158–175, 1995, doi: 10.1109/34.368173.

[90] S. J. Osher and F. Santosa, “Level Set Methods for Optimization Problems Involving Geometry and Constraints I. Frequencies of a Two-Density Inhomogeneous Drum,” *J. Comput. Phys.*, vol. 171, no. 1, pp. 272–288, Jul. 2001, doi: 10.1006/jcph.2001.6789.

[91] C. Li, R. Huang, Z. Ding, J. C. Gatenby, D. N. Metaxas, and J. C. Gore, “A level set method for image segmentation in the presence of intensity inhomogeneities with application to MRI,” *IEEE Trans. Image Process.*, vol. 20, no. 7, pp. 2007–2016, Jul. 2011, doi: 10.1109/TIP.2011.2146190.

[92] J. A. Sethian and A. Wiegmann, “Structural Boundary Design via Level Set and Immersed Interface Methods,” *J. Comput. Phys.*, vol. 163, no. 2, pp. 489–528, Sep. 2000, doi: 10.1006/jcph.2000.6581.

[93] J. A. Sethian and P. Smereka, “Level set method for fluid interfaces,” *Annu. Rev. Fluid Mech.*, vol. 35, no. 1, pp. 341–372, Jan. 2003, doi: 10.1146/annurev.fluid.35.101101.161105.

[94] X. B. Duan, Y. C. Ma, and R. Zhang, “Shape-topology optimization for Navier-Stokes problem using variational level set method,” *J. Comput. Appl. Math.*, vol. 222, no. 2, pp. 487–499, Dec. 2008, doi: 10.1016/j.cam.2007.11.016.

[95] W. Yue, C. L. Lin, and V. C. Patel, “Numerical simulation of unsteady multidimensional free surface motions by level set method,” *Int. J. Numer. Methods Fluids*, vol. 42, no. 8, pp. 853–884, Jul. 2003, doi: 10.1002/fld.555.

[96] J. Vidale, “Finite-difference calculation of travel times,” *Bull. Seismol. Soc. Am.*, vol. 78, no. 6, pp. 2062–2076, Dec. 1988.

[97] F. Qin, Y. Luo, K. B. Olsen, W. Cai, and G. T. Schuster, “Finite-difference solution of the eikonal equation along expanding wavefronts,” *Geophysics*, vol. 57, no. 3. pp. 478–487, 1992, doi: 10.1190/1.1443263.

[98] Y. H. Tsai, Y. Giga, and S. Osher, “A level set approach for computing discontinuous solutions of Hamilton-Jacobi equations,” *Math. Comput.*, vol. 72, no. 241, pp. 159–182, Aug. 2003, doi: 10.1090/S0025-5718-02-01438-2.

[99] S. Osher and R. P. Fedkiw, “Level Set Methods: An Overview and Some Recent Results,” *J. Comput. Phys.*, vol. 169, no. 2, pp. 463–502, May 2001, doi: 10.1006/JCPH.2000.6636.

[100] K. Unami, O. Mohawesh, and R. M. Fadhil, “Time periodic optimal policy for operation of a water storage tank using the dynamic programming approach,” *Appl. Math. Comput.*, vol. 353, pp. 418–431, Jul. 2019, doi: 10.1016/J.AMC.2019.02.005.

[101] L. R. Perera *et al.*, “Towards establishing a system of monitoring and evaluation for participatory irrigation management and development program in Cambodia,” *IWMI Rep. to AFD, Colombo*, pp. 1–35, 2007.

[102] H. C. Thoeun, “Observed and projected changes in temperature and rainfall in Cambodia,” *Weather Clim. Extrem.*, vol. 7, pp. 61–71, Mar. 2015, doi: 10.1016/j.wace.2015.02.001.

[103] A. H. M. B. Alam, K. Unami, and M. Fujihara, “Holistic water quality dynamics in rural artificial shallow water bodies,” *J. Environ. Manage.*, vol. 223, pp. 676–684, Oct. 2018, doi: 10.1016/j.jenvman.2018.06.076.

[104] W. R. McMinn, Q. Yang, and M. Scholz, “Classification and assessment of water bodies as adaptive structural measures for flood risk management planning,” *J. Environ. Manage.*, vol. 91, no. 9, pp. 1855–1863, Sep. 2010, doi: 10.1016/j.jenvman.2010.04.009.

[105] E. F. Toro and P. Garcia-Navarro, “Godunov-type methods for free-surface shallow flows: A review,” *J. Hydraul. Res.*, vol. 45, no. 6, pp. 736–751, 2007.

[106] H. M. Zhang, “A non-equilibrium traffic model devoid of gas-like behavior,” *Transp. Res. Part B Methodol.*, vol. 36, no. 3, pp. 275–290, 2002.

[107] J. McCrea and S. Moutari, “A hybrid macroscopic-based model for traffic flow in road networks,” *Eur. J. Oper. Res.*, vol. 207, no. 2, pp. 676–684, 2010.

[108] V. R. Ambati and O. Bokhove, “Space–time discontinuous Galerkin discretization of rotating shallow water equations,” *J. Comput. Phys.*, vol. 225, no. 2, pp. 1233–1261, 2007.

[109] M. Burger, S. Göttlich, and T. Jung, “Derivation of a first order traffic flow model of Lighthill-Whitham-Richards type,” *IFAC-PapersOnLine*, vol. 51, no. 9, pp. 49–54, 2018.

[110] R. Bürger and W. L. Wendland, “Sedimentation and suspension flows: Historical perspective and some recent developments,” *J. Eng. Math.*, vol. 41, no. 2, pp. 101–116, 2001.

[111] G. Chen, R. Pan, and S. Zhu, “Singularity formation for the compressible Euler equations,” *SIAM J. Math. Anal.*, vol. 49, no. 4, pp. 2591–2614, 2017.

[112] A. Corli and L. Malaguti, “Wavefronts in traffic flows and crowds dynamics,” in *Anomalies in Partial Differential Equations*, Springer, 2021, pp. 167–189.

[113] W. L. Jin, Q. J. Gan, and J. P. Lebacque, “A kinematic wave theory of capacity drop,” *Transp. Res. Part B Methodol.*, vol. 81, pp. 316–329, 2015, doi: https://doi.org/10.1016/j.trb.2015.07.020.

[114] W. L. Jin, “Continuous kinematic wave models of merging traffic flow,” *Transp. Res. Part B Methodol.*, vol. 44, no. 8, pp. 1084–1103, 2010, doi: https://doi.org/10.1016/j.trb.2010.02.011.

[115] K. Han, B. Piccoli, and W. Y. Szeto, “Continuous-time link-based kinematic wave model: formulation, solution existence, and well-posedness,” *Transp. B Transp. Dyn.*, vol. 4, no. 3, pp. 187–222, 2016.

[116] J. Li, X. Guo, and L. Zhao, “High-efficiency calculation method for watershed rainfall-runoff routing using one-dimensional dynamic wave equations,” *J. Mt. Sci.*, vol. 14, no. 10, pp. 2097–2105, 2017.

[117] O. A. Oleinik, “Discontinuous solutions of non-linear differential equations,” *Uspekhi Mat. Nauk*, vol. 12, pp. 3–73, 1956.

[118] S. N. Kružkov, “First order quasilinear equations in several independent variables,” *Math. USSR-Sbornik*, vol. 10, no. 2, pp. 217–242, 1970.

[119] Z. Q. Shao, Y. C. Li, and D. X. Kong, “Global weakly discontinuous solutions to quasilinear hyperbolic systems of conservation laws with damping with a kind of non-smooth initial data,” *Zeitschrift für Angew. Math. und Phys.*, vol. 59, no. 6, pp. 935–968, 2008.

[120] L. Wang, “Global existence of weak discontinuous solutions to the Cauchy problem with small BV initial data for quasilinear hyperbolic systems,” *Math. Methods Appl. Sci.*, vol. 38, no. 5, pp. 966–979, 2015.

[121] A. Jeffrey, “The evolution of discontinuities in solutions of homogeneous nonlinear hyperbolic equations having smooth initial data,” *J. Math. Mech.*, vol. 17, no. 4, pp. 331–352, 1967.

[122] A. Jeffrey, “Mathematical Methods in Wave Propagation: Part II--Non-Linear Wave Front Analysis,” *Int. J. Mathamatical Educ. Sci. Technol.*, vol. 2, no. 1, pp. 5–16, 1971.

[123] A. Jeffrey and A. Donato, “The occurrence of singularities in solutions of homogeneous systems of two first order quasilinear hyperbolic equations with smooth initial data,” *Wave motion*, vol. 1, no. 3, pp. 177–185, 1979.

[124] G. M. Coclite, M. Garavello, and B. Piccoli, “Traffic flow on a road network,” *SIAM J. Math. Anal.*, vol. 36, no. 6, pp. 1862–1886, 2005.

[125] S. Chen, “How does a shock in supersonic flow grow out of smooth data?,” *J. Math. Phys.*, vol. 42, no. 3, pp. 1154–1172, 2001.

[126] M. G. Crandall and A. Majda, “Monotone difference approximations for scalar conservation laws,” *Math. Comput.*, vol. 34, no. 149, pp. 1–21, 1980.

[127] G. Bretti, R. Natalini, and B. Piccoli, “Numerical approximations of a traffic flow model on networks,” *Networks Heterog. Media*, vol. 1, no. 1, pp. 57–84, 2006.

[128] U. S. Fjordholm and S. Mishra, “Accurate numerical discretizations of non-conservative hyperbolic systems,” *ESAIM Math. Model. Numer. Anal. Mathématique Anal. Numérique*, vol. 46, no. 1, pp. 187–206, 2012.

[129] R. A. Adams and J. J. F. Fournier, *Sobolev spaces*. Amsterdam: Elsevier, 2003.

[130] D. Gąsiorowski and T. Kolerski, “Numerical Solution of the Two-Dimensional Richards Equation Using Alternate Splitting Methods for Dimensional

Decomposition," *Water*, vol. 12, no. 6, p. 1780, 2020.

[131] C. Hirsch, *Numerical computation of internal and external flows. Vol. 2-Computational Methods for Inviscid and Viscous Flows*. John Wiley & Sons, Ltd., 1990.

[132] W. Ressel, A. Wolff, S. Alber, and I. Rucker, "Modelling and simulation of pavement drainage," *Int. J. Pavement Eng.*, vol. 20, no. 7, pp. 801–810, 2019.

[133] F. van Wageningen-Kessels, W. Daamen, and S. P. Hoogendoorn, "Two-dimensional approximate Godunov scheme and what it means for continuum pedestrian flow models," *Transp. Sci.*, vol. 52, no. 3, pp. 547–563, 2018.

[134] K. Unami, R. M. Fadhil, and O. Mohawesh, "Bounding linear rainfall-runoff models with fractional derivatives applied to a barren catchment of the Jordan Rift Valley," *J. Hydrol.*, vol. 593, p. 125879, 2021.

[135] P. Rao, "Numerical modeling of open channel flows with moving fronts using a variable boundary formulation," *Appl. Math. Comput.*, vol. 182, no. 1, pp. 369–382, 2006.

[136] B. Chentouf and N. Smaoui, "Stability analysis and numerical simulations of a one dimensional open channel hydraulic system," *Appl. Math. Comput.*, vol. 321, pp. 498–511, 2018.

[137] A. Sukhtayev, Z. Yang, and K. Zumbrun, "Spectral stability of hydraulic shock profiles," *Phys. D Nonlinear Phenom.*, vol. 405, 2020.

[138] S. Jerez and M. Arciga, "Switch flux limiter method for viscous and nonviscous conservation laws," *Appl. Math. Comput.*, vol. 246, pp. 292–305, 2014.

[139] J. Glaubitz, “Shock capturing by Bernstein polynomials for scalar conservation laws,” *Appl. Math. Comput.*, vol. 363, 2019.

[140] R. M. Fadhil and K. Unami, “A multi-state Markov chain model to assess drought risks in rainfed agriculture: a case study in the Nineveh Plains of Northern Iraq,” *Stoch. Environ. Res. Risk Assess.*, pp. 1–21, 2021.

[141] M. G. Crandall and P. L. Lions, “Two approximations of solutions of Hamilton-Jacobi equations,” *Math. Comput.*, vol. 43, no. 167, pp. 1–19, Sep. 1984, doi: 10.1090/s0025-5718-1984-0744921-8.

[142] P. L. Lions, “Optimal control of diffusion processes and Hamilton–Jacobi–Bellman equations part 2: viscosity solutions and uniqueness,” *Commun. Partial Differ. equations*, vol. 8, no. 11, pp. 1229–1276, 1983.

[143] G. Barles and B. Perthame, “Exit time problems in optimal control and vanishing viscosity method,” *SIAM J. Control Optim.*, vol. 26, no. 5, pp. 1133–1148, 1988.

[144] A. I. Subbotin, *Generalized Solutions of First Order PDEs - The Dynamical Optimization Perspective*. Birkhäuser, Basel, 1995.

[145] K. H. Karlsen and N. H. Risebro, “A note on front tracking and the equivalence between viscosity solutions of Hamilton-Jacobi equations and entropy solutions of scalar conservation laws.,” *Nonlinear Anal. Theory, Methods Appl.*, pp. 455–469, 2002.

[146] K. Unami and O. Mohawesh, “A unique value function for an optimal control problem of irrigation water intake from a reservoir harvesting flash floods,” *Stoch. Environ. Res. Risk Assess.*, vol. 32, no. 11, pp. 3169–3182, 2018.

[147] M. H. Chaudhry, *Open-channel flow*. New York: Springer Science & Business Media,

2008.

[148] H. B. Keller, *Numerical methods for two-point boundary-value problems*. New York: Courier Dover Publications, 2018.